MASTER THESIS

3D Transient and Crystallization model for Laser Assisted Tape Winding

Author:
Victor HOEKSEMA

Supervisor:
Dr. I. BARAN

Chairman:
Prof.dr.ir. R. AKKERMAN

External Member:
Dr.ir. E.S. PERDAHCIOĞLU

A thesis submitted in fulfillment of the requirements for the degree of Master of Science in Mechanical Engineering

Production Technology
Faculty of Engineering Technology

November 21, 2017

UNIVERSITY OF TWENTE.

UNIVERSITY OF TWENTE

Abstract

Faculty of Engineering Technology
Production Technology

Master of Science in Mechanical Engineering

3D Transient and Crystallization model for Laser Assisted Tape Winding

by Victor HOEKSEMA

The utilisation of fibre-reinforced polymers (FRP) has grown considerably, especially in the automotive and aerospace industries. Laser Assisted Tape Winding (LATW) is one of the production methods that utilises FRP to fabricate parts with complex shapes, great strength and with little weight.

The LATW additive manufacturing process winds uni-directional (UD) thermoplastic prepreg tape on a rotation mandrel, while a laser heats the tape and a roller pressurises the tape to consolidate layers to the mandrel. A tubular product is fabricated by consolidating multiple layers on the mandrel using complex winding patterns.

Currently, LATW does not achieve the same material quality of techniques that use post processes. This requires investigation of the in-situ consolidation that occurs during tape winding. Therefore the in-situ consolidation is investigated by simulating the process with a three-dimensional Lagrangian transient kinematic-optical-thermal(KOT) model. Using the KOT model it will be possible to determine the temperature evolution of each layer for all windings. This will allow for a complete temperature history of the LATW process. The temperature history is then analyzed to predict the crystallinity growth of the substrate in through-thickness and width direction. This prediction is made using a crystallinity model for Carbon/PEEK tape that analyses the heating and cooling rates in thermal history.

Experimental validation was carried for both models by using thermal and crystallinity measurements. The experimental measurements and the KOT simulation showed only minor differences in thermal history, thus validating one another. Using differential scanning calorimetry(DSC) measurements and the crystallization model we explain the through-thickness crystallinity difference of the laminate. Lower crystallinity values at the bottom and top are explained due to high conduction rates and fewer temperature cycles respectively as well as an existence of an initial crystallinity value after melt.

The three-dimensional Lagrangian transient KOT model was also used to investigate the change in temperature due to effects of transverse boundary conditions. This was performed using a reduction of the transverse complexity in width direction. Additional simulation were performed to determine the consequences of lay-up and geometry on the heating and cooling cycle. This was studied with different: tape widths, mandrel radius's, mandrel materials, environment temperatures and substrate fibre-orientations to determine the effect on nip-point temperature and crystallinity.

Acknowledgements

I would like to thank my professor Ismet Baran for the guidance during the project, S. Mohammad A. Hosseini for reviewing my work and being a great discussion partner during our weekly meetings, the members of the committee Remco Akkerman and Semih Perdahcioğlu for being available for the colloquium on such a short date, my lovely girlfriend Tessa Ezendam and mother Marga Houwers for continuous support and I'm especially grateful to my brother Harm Hoeksema for checking my work and pushing me to write pages.

I also like to thank the following teachers and staff from my Faculty and Department that played an important role in my study: Ton Bor, Laurent Warnet, Ivo Vrooijink, Debbie Zimmerman and Marcel Ellenbroek.

Contents

Abstract iii

Acknowledgements v

1 Introduction 1
- 1.1 Motivation . . . 2
- 1.2 Laser Assisted Tape Winding . . . 2
  - 1.2.1 Machine set-up . . . 3
  - 1.2.2 Applications . . . 4
- 1.3 Research context . . . 5
  - 1.3.1 ambliFibre project . . . 5
  - 1.3.2 Previous work . . . 5
- 1.4 Objective . . . 6
  - 1.4.1 Research question . . . 6
  - 1.4.2 Scope . . . 6
  - 1.4.3 Methodology . . . 8

2 Thermal Model 9
- 2.1 Setup of the Thermal Model . . . 9
  - 2.1.1 Assumptions . . . 9
  - 2.1.2 Lagrangian Coordinate system . . . 10
  - 2.1.3 Transient analyses . . . 11
  - 2.1.4 Two-dimensional model . . . 12
  - 2.1.5 Three-dimensional model . . . 12
- 2.2 Solution Structure . . . 13
  - 2.2.1 Birth-and-death of Elements . . . 13
  - 2.2.2 Initial Condition Method . . . 13
- 2.3 Simulation Parameters . . . 13
  - 2.3.1 Global simulation parameters . . . 14
- 2.4 Boundary Conditions . . . 15
- 2.5 Mesh and Step Parameters . . . 16
- 2.6 Material Properties . . . 16
  - 2.6.1 Polymer Matrix System . . . 17
  - 2.6.2 Degradation and decomposition . . . 17
  - 2.6.3 Temperature depended material . . . 18
- 2.7 Energy Balance . . . 18
  - 2.7.1 One-dimensional thermal problem . . . 18
  - 2.7.2 Three-dimensional thermal problem . . . 19
- 2.8 Optical-Thermal Model . . . 20
  - 2.8.1 Effect of conduction in winding direction . . . 20
- 2.9 Kinematic-Optical-Thermal Model . . . 21
- 2.10 Simulation Setup . . . 22
  - 2.10.1 Simulation Settings . . . 22
  - 2.10.2 Process Simulation . . . 23
- 2.11 Model Reduction . . . 25
- 2.12 Simulation Options . . . 25
  - 2.12.1 Model case study . . . 26

2.12.2 Variation in tape width and radius . . . 27
2.12.3 Lay-up build up . . . 27
2.12.4 Adjacent windings . . . 27
2.12.5 Mandrel Material . . . 27
2.12.6 Environment Temperature . . . 28

3 Crystallinity Model **29**
3.1 Crystallinity . . . 29
3.2 Crystallinity based on Cooling Rate . . . 30
3.3 Cooling rate in LATW . . . 31
3.4 Crystallinity based on phase transition . . . 32
3.5 Crystallinity based on Cooling rate and Enthalpy . . . 33

4 Experiments **35**
4.1 LATW Specimens . . . 35
4.2 Thermocouple results . . . 36
4.2.1 Temperature development of experiments and simulations . . . 37
4.2.2 Trend of peak temperatures in continuous hoop winding . . . 37
4.2.3 Environment difference between experiments and simulation 38
4.3 Crystallinity measurements . . . 38
4.3.1 Crystallinity results . . . 39
4.3.2 Crystallinity change per position . . . 40

5 Simulation Study **43**
5.1 Model Case Study . . . 43
5.1.1 Reduction in the adjacent winding model . . . 43
5.1.2 Adjacent winding compared to hoop winding model . . . 44
5.1.3 Hoop winding model influence of substrate . . . 44
5.1.4 No transverse convection and conduction . . . 44
5.2 Variation in tape width . . . 45
5.3 Variation in radius . . . 46
5.3.1 Radius effect on hoop winding . . . 46
5.3.2 Radius effect on adjacent winding . . . 47
5.4 Mandrel material . . . 48
5.5 Thermal Degradation . . . 48
5.6 Variation in environment temperature . . . 49
5.7 Substrate Fibre-orientation . . . 50
5.8 Evaluation . . . 51

6 Conclusions and Recommendations **53**
6.1 Conclusions . . . 53
6.2 Recommendations . . . 54
6.2.1 Stress-Strain Model . . . 54
6.2.2 After-treatment . . . 54
6.2.3 Winding Angle . . . 54
6.2.4 3D Transient model, no conductivity in placement direction . 54
6.2.5 Laser melt model . . . 54

Bibliography **55**

A Method Comparison in LATP 3D simulation **57**
A.1 3D Kinematic-Optical-Model for placement . . . 57
A.1.1 Volume Solid70 elements . . . 57
A.1.2 Section Shell131 elements . . . 58
A.2 Method Comparison . . . 59

B ANSYS Thermal Equations **61**
B.1 Heat flow Fundamentals . . . 61
B.1.1 First law of thermodynamics . . . 61
B.1.2 Boundary Conditions . . . 62
B.1.3 Derivation of Heat flow Matrices . . . 62
B.2 Element Settings . . . 64
B.3 Convergence tolerances . . . 64

C Constraint eq between shell elements **65**

D Reduced Model Validation **67**

E Temperature depended material **69**
E.1 Material Study . . . 69
E.2 Simulation results . . . 69
E.2.1 longitude, Transverse conductivity and Density . . . 69
E.2.2 Through thickness conductivity . . . 69
E.2.3 Heat Capacity . . . 70

List of Figures

1.1 Laser AssistedExamples . . . 1
1.2 LATW Machine Setup . . . 2
1.3 LATW-Schematic . . . 3
1.4 Laser Assisted Examples . . . 4
1.5 LATW-Schematic . . . 5
1.6 Full Process Simulation Model . . . 7
1.7 Full Process Simulation Model . . . 7
1.8 Methodology schematic . . . 8

2.1 Lagrangian model . . . 10
2.2 Compare Transient and Steady state . . . 11
2.3 Eulerian approach . . . 12
2.4 Angular Winding . . . 12
2.5 Solution Structures . . . 13
2.6 Boundary Conditions . . . 15
2.7 Fibre-matrix scale . . . 16
2.8 Phase Diagram . . . 17
2.9 Mer units of PEEK . . . 17
2.10 Two-dimensional Simulation Model . . . 20
2.11 Two-dimensional simulation . . . 20
2.12 KOT simulation settings . . . 21
2.13 Coupling of SHELL131 . . . 22
2.14 Terminology difference between windings and layers . . . 23
2.15 KOT model simulation schematic . . . 24
2.16 Model size reduction . . . 25
2.17 Model case study's . . . 26
2.18 Adjacent windings . . . 27

3.1 Typical DSC chart . . . 30
3.2 Crystallinity as a function of cooling rate . . . 30
3.3 Temperature history curve . . . 31
3.4 Cooling rate curve of the 6th layer . . . 31
3.5 Peak crystallisation times of PEEK . . . 32
3.6 Crystallisation rate of Carbon-PEEK. . . . 33

4.1 Aluminium mandrels for tape winding . . . 35
4.2 First layer thermocouples measurements with a radius of 122mm. . . . 36
4.3 First layer thermocouples measurements with a radius of 212mm. . . . 36
4.4 General curve difference . . . 37
4.5 Trend change in thermocouples measurements and simulation results 37
4.6 Temperature change in equipment . . . 38
4.7 DSC Material and Equipement . . . 38
4.8 DSC curve for the 122mm radius ring. . . . 39
4.9 DSC curve for the 212mm radius ring . . . 39
4.10 Crystallinityresultsim . . . 40

5.1 Reduction in adjacent winding model . . . 43

5.2 Change in Boundary Conditions in transverse direction 44
5.3 Nip-point temperature in transverse direction 45
5.4 Cooling difference between center and edge 46
5.5 Mandrel temperature, hoop winding mandrel model 46
5.6 Substrate temperature, mandrel acts as a heat sink 47
5.7 Radius change in adjacent winding 47
5.8 Effect of mandrel material on LATW 48
5.9 Effect of Environment Temperature on LATW 49
5.10 Influence by Lay-up on thermal history 50

A.1 LATP with Solid70 57
A.2 LATP with Shell 58

B.1 Shell 131 Element 64

C.1 Coupling of SHELL131 65

D.1 Nip-point temperatures, KOT adjacent 3B model 67
D.2 Themperature history, full and reduced perimeter, KOT adjacent 3B model 67

E.1 Material Study: Temperature 70
E.2 Material Study: Heating and Cooling Rate 70

List of Tables

2.1 Global simulation parameters 14
2.2 Boundary conditions 15
2.3 Mesh Simulation Parameters 16
2.4 Temperature dependent material properties 18

4.1 Small radius DSC Results 40
4.2 Large radius DSC Results 40

5.1 Nip-point temperature and Crystallinity by different environment temperatures 45
5.2 Mandrel material properties 48
5.3 Nip-point temperature and Crystallinity by different environment temperatures 49
5.4 Crystallinity of multiple width positions with different substrate fibre-orientations 50

A.1 Method and Element comparison 59

List of Abbreviations

FRP	**F**ibre-**R**einforced **P**olymers
FW	**F**ilament **W**inding
AP	**A**utomated **F**ibre **P**lacement
ATL	**A**utomated **T**ape **L**aying
LATW	**L**aser **A**ssisted **T**ape **W**inding
LATP	**L**aser **A**ssisted **T**ape **P**lacement
UD	**U**ni-**D**irectional
APDL	**A**NSYS **P**arametric **D**esign **L**anguage
CFD	**C**omputational **F**luid **D**ynamics
IC	**Í**nitial **C**ondition
B&D	**B**irth and **D**eath
PEEK	**P**oly-**E**ther-**E**ther-**K**etone
KOT	**K**inematic-**O**ptical-**T**hermal KOT
TTOP	**T**emperature **Top**
TE	**T**emperature **E**lement Position
TBOT	**T**emperature **Bot**tom
DSC	**D**ifferential **S**canning **C**alorimetry
IR	**I**nfrared **S**pectroscopy
NMR	**N**uclear **M**agnetic **R**esonance

Chapter 1

Introduction

In recent years, the influence in the usage of composite materials has grown significantly especially in the multi-billion dollar automotive and aerospace industries. The reason behind this growth is the need for weight reduction as well as the advancement in composite production methods[1]. Composite materials commonly used are Fibre-reinforced polymers (FRP), which consists of a polymer matrix reinforced with fibres, e.g. carbon or glass. Using innovative composite production methods it is possible to fabricate parts in complex shapes while combining great strength with little weight allowing for a 'best of both worlds'.

The advanced production method discussed in this thesis uses Thermoplastic Polymers - an emerging sub-group of matrix materials. Their main benefit is that the fibre reinforced thermoplastic may be processed repeatedly: by bringing the matrix above its melting temperature. In the process of remelting the material allows for the recyclability and the application of a variety of possible additive manufacturing techniques, such as Filament Winding (FW), Automated Fibre Placement (AP), Automated Tape Laying (ATL) and Laser Assisted Tape Winding (LATW). The latter technique, LATW, is the focus of this thesis out of the various additive manufacturing techniques.

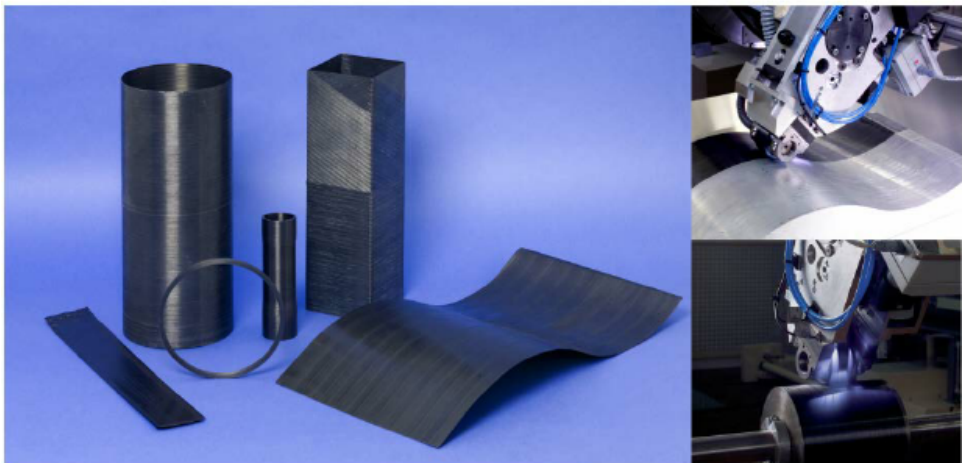

FIGURE 1.1: Tape Placement and Winding Examples

1.1 Motivation

Laser Assisted Tape Winding is a cost-effective technique, to create composite tubular shapes. The tubular shapes are created by winding high-quality unidirectional composite tape around a mandrel and consolidates the tape with a roller and laser. The roller and laser provide respectively pressure and heat, this eliminates the need for extensive and expensive post-processes such as high-pressure consolidation with an autoclave[2]. Since there is no post-processes consolidation the consolidation that occurs during the process is, therefore the main factor for the bonding and material quality. Currently, LATW does not achieve the same material quality of techniques that use post processes. This requires investigation of the in-situ consolidation that occurs during tape winding. Since experimental investigating requires significant costs and time, we make the choice to investigate by creating a simulation model. The created simulation model should be validated using experimental results. In this study the consolidation is investigated by simulating the process using a 3D Lagrangian Transient Simulation model, the choices for this model are explained in chapter 2.

1.2 Laser Assisted Tape Winding

Laser Assisted Tape Winding (LATW) consists of four primary mechanisms: the rotating mandrel on which the tape will be placed (in other techniques this is similar to a mould), the tape feeding unit that places and the cuts tape, a roller that puts pressure on the tape for bonding between the layers and finally the laser that heats the tape to melting temperature. An example of the machine setup is depicted in figure 1.2[1]

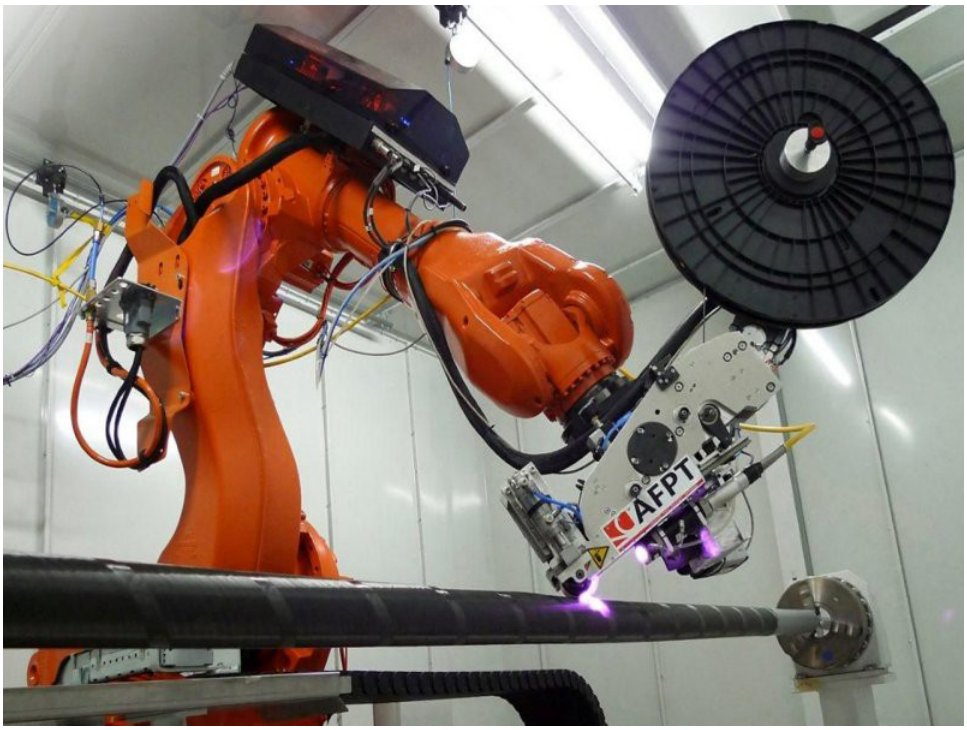

FIGURE 1.2: LATW Machine Setup

[1]Source: University of Siegen

1.2.1 Machine set-up

Winding tape around the mandrel forms a layer, when a layer is placed on the substrate it consolidates with the layer underneath, because of the pressure from the roller and heat of the laser. This consolidation occurs at nip-point, see the schematic in figure 1.3. The mandrel will determine the basic form of the end product by winding tape around the mandrel. After consolidating all the layers of tape on the mandrel then is the LATW process finished without the need for further post-process consolidation. The final product can be removed from the mandrel or left on the mandrel if the goal is to reinforce the mandrel, such as the case when the mandrel is a pipe or pressure vessel.

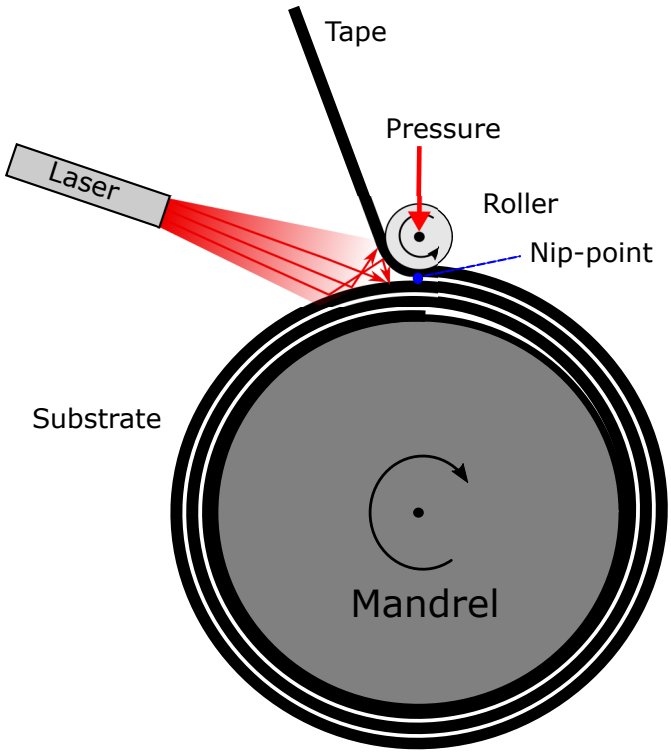

FIGURE 1.3: LATW-Schematic

The strength of the final product is determined by the direction of the tape, laminate thickness, bonding strength, mechanical and temperature depended material properties. Bonding strength regards to the consolidation of the multiple layers, the mechanical material properties refer to the strength of the layers, and temperature dependent material properties refer to the crystallinity and thermal degradation. The focus on this specific LATW research is improving the temperature depended material properties by investigating the heating and cooling region that occur respectively before and after nip-point.

1.2.2 Applications

Tape winding is already being used in a few application, figure 1.4 illustrates a few possibilities. Figure 1.4a[2] shows several pipes made of carbon-reinforced polyamide12/carbon fibre, which could be used for subsea applications in mainly the oil and gas industry. Compared to the steel equivalents, these provide excellent mechanical properties and corrosion resistance, at a low weight. Figure 1.4b[3] Thermoplastics pressure vessels of 300-liter water storage tank using E-CR glass SE4220 and figure 1.4c[4] shows automated tape layup being used to create the all-carbon composite fuselage of the Hawker Beechcraft Hawker 4000 business jet.

(A) Pipes

(B) Pressure vessel

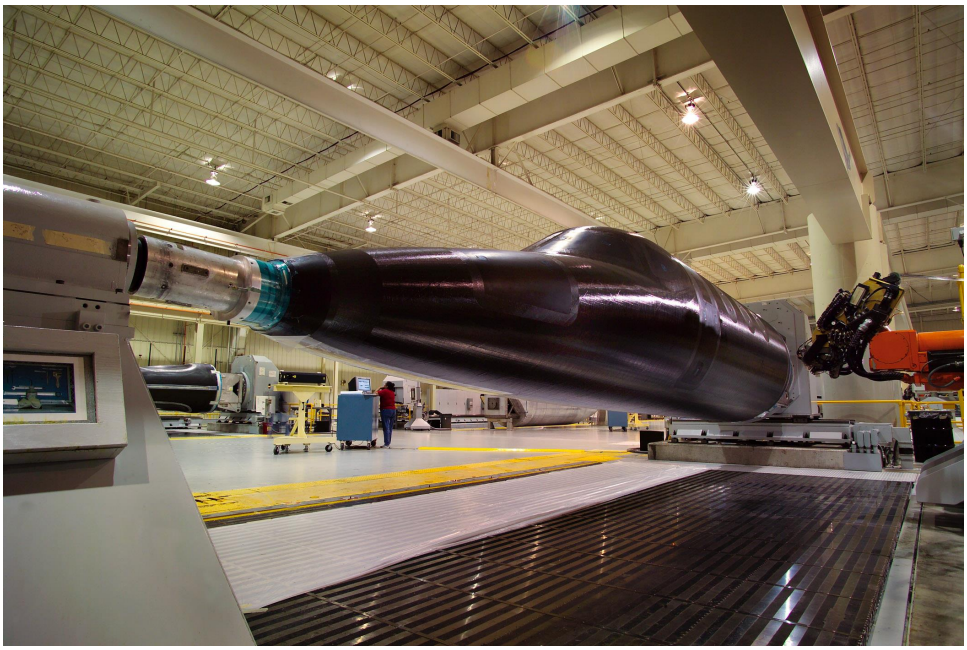

(C) composite fuselage

FIGURE 1.4: Laser Assisted Examples

[2] aSource: Fraunhofer IPT. Retrieved from: article[3]
The vessel and fuselage depicted here was produced using a non-laser-assisted winding method
[3] bSource: JEC Europe. Retrieved from: http://www.compositesworld.com/
[4] cSource: Photo courtesy Hawker Beechcraft. Retrieved from: http://www.mmsonline.com/

1.3 Research context

1.3.1 ambliFibre project

ambliFibre has the goal to develop and validate the first intelligent model-based controlled laser-assisted tape winding system for fibre-reinforced thermoplastic (FRP) components serving the needs of tomorrow's energy production and storage with an enhanced reliability, flexible, easily manageable and cost-efficient manufacturing technology[4]

Thus ambliFibre aims at fulfilling this demand by improving the diode laser-assisted tape winding process, systems and assisting software solutions to enable an efficient and flexible production for such advanced tubular composite products out of thermoplastic unidirectional (UD) fibre-reinforced pre-impregnated raw stock material, also called prepreg or tape[5].

The research conducted in this thesis will be to assist the ambliFibre project.

1.3.2 Previous work

Extensive work has been done to the closely-related laser-assisted tape placement (LATP) and the LATW process, such as previous efforts by Grouve [6] and Reichardt[7] here at the University of Twente. The difference between LATW and LATP is that in the latter case, tape is placed on a flat surface instead of being wound around a mandrel, however underlying physics and mechanisms are almost equal.

Grouve[6] developed a one-dimensional transient thermal model to predict the temperature of both tape and substrate for the LATP process for flat substrates. Reichardt[7] continued with the model, and developing a numerical optical model as well as a semi-analytical optical-thermal model. These models allow for non-uniform laser power distribution and have a micro-model to account for the non-specular reflection of flat and singly-curved substrates, see figure 1.5. Kim[8] developed a 2D Lagrangian fully transient[8] and 2D Eulerian quasi-steady state model[9] for which the transient model had better prediction compared to the experimental results. Toso[10] developed a 3D steady-state model, that performs multiple steady-state simulations for each layer to predict transient results for torch heated tape winding, with experimental results for validation.

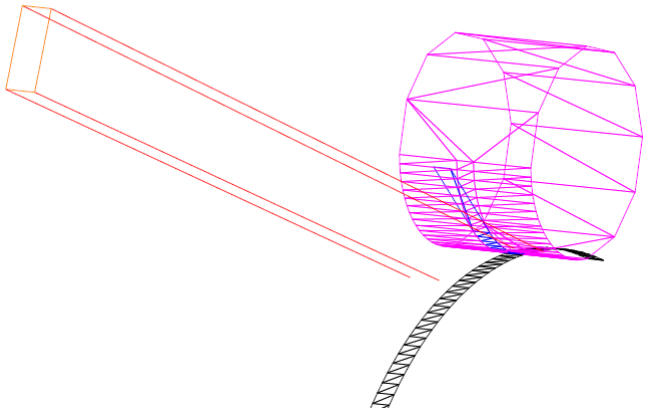

FIGURE 1.5: Matlab Tool LATW

1.4 Objective

The objective is to predict temperature history and crystallinity using a comprehensive kinematic-optical-thermal(KOT) model.

Using the KOT model it will be possible to determine the temperature evolution of each layer for all windings. This will allow for a complete temperature history of the LATW process. The temperature history is then analyzed to predict the crystallinity growth of the substrate in through-thickness and width direction.

Kinematic model refers to time depended geometry, for which a piece of tape is wound in each time step. The optical part refers to the geometry based reflection data for which the heat flux of the laser is implemented. The thermal model refers to the equations that are solved, to obtain the full temperature history.

1.4.1 Research question

To help realize the objective, this thesis will focus on answering the following research questions:

Prediction of the temperature depended material properties based on the heating and cooling history during manufacturing. Fibre-reinforced thermoplastic allows for remelting of the matrix material while keeping the fibres intact. During the LATW production process, the tape is continuously wound. With tape and substrate being reheated to above glass transition and melt temperatures, resulting in multiple heating and cooling cycles. Change in crystallinity can easily occur during such cycles, as well as the occurrence of material degradation for temperatures above melt.

Investigation of change in temperature history, as a result of transverse boundary conditions in width direction. By researching the transverse convections and conductions in width direction. it is possible to determine which effects can be neglected in future simulations, and which conditions affect temperature history the most.

The consequences of lay-up on the heating and cooling cycle. Winding with different fibre-orientations can have a large effect on the interface interactions. Two factors about this subject are discussed in this thesis: heat absorption of the substrate and accumulated heat in the substrate and mandrel. Consequences are determined for hoop winding and adjacent tape winding.

1.4.2 Scope

To produce a high-quality composite part with LATW the full process simulation model is illustrated in figure 1.6 as a flowchart. This process has been set-up to try and include all models related to the quality of a LATW product. Following models are specified in the flowchart:

1. Part design: specified to tape winding
2. Kinematic model: that calculates the winding paths based on the geometry
3. Optical model: determines the reflections based on the winding paths
4. Thermal model: for the correct temperature at nip-point
5. Mechanical model: to determine the strains at the roller interaction, while taking into account temperature based material behaviour.
6. Crystallinity model: predicts the crystallinity growth using the thermal history.
7. Bonding model: specifically determines the bonding quality of the tape and substrate.

8. Quality analyses: to be able to regulate the final material properties and weak points or damages in the designed part.

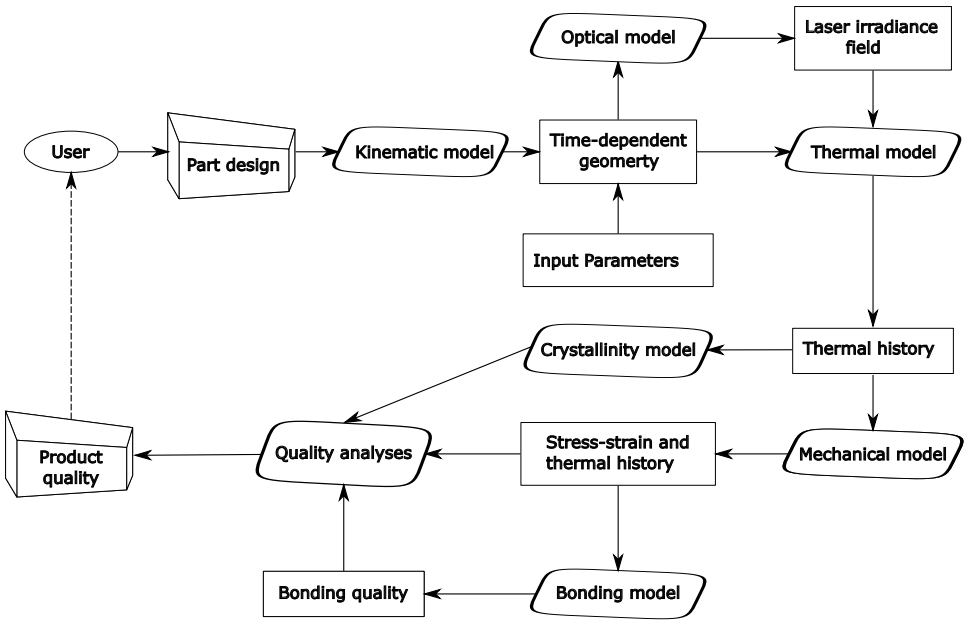

FIGURE 1.6: Full Process Simulation Model

Implementation of the full process simulation model is beyond the scope of this study, so in this research reduces the scope by focussing on the temperature history and the temperature dependent material properties; crystallinity and thermal degradation. Reducing the scope only to temperature effects will allow for the study of the temperature depended product quality to be more in-depth. The flowchart of the reduced process simulation model is illustrated in figure 1.7. In the reduced process simulation model the following is changed as compared to figure 1.6:

- The mechanical and bonding models are removed
- The optical model is changed to optical settings since the currently available optical data is only geometry based and not time dependent.
- Product quality is changed to Temperature-depended product quality, since mechanical material properties are not taken into account in this study.
- Part Design is changed to Input Parameters, this allows for first analyzing simple geometries such as flat and cylindrical surfaces.

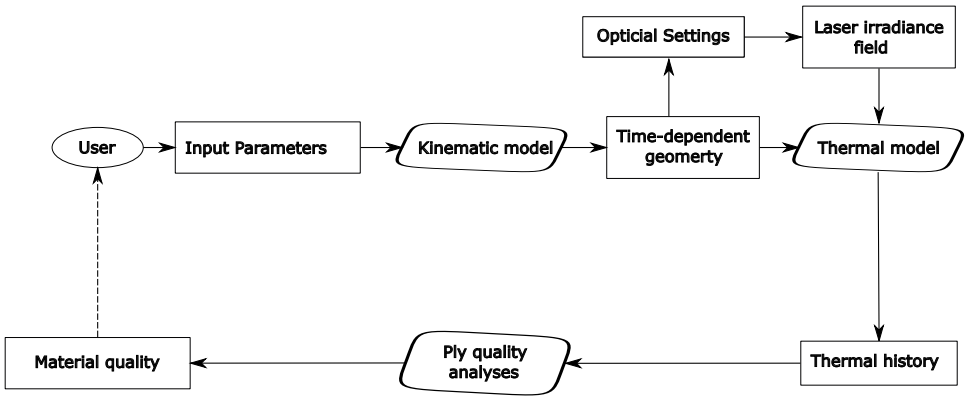

FIGURE 1.7: Reduced Process Simulation Model

1.4.3 Methodology

The methodology consists of a variety of steps along with the usage of different computer programs. The focus of the simulation model is to determine the temperature history through the thickness, after tape placement. A schematic overview is visible in figure 1.8.

1. In the first step, we continue with the optical model created by Reichardt[7], as well as non-linear thermal orthotropic material data for the AS4/PEEK 61% composite tape.
2. Tape winding is then simulated using the commercially available finite element package of 'ANSYS 17.0 APDL'. This finite element model simulates winding patterns and has optical heat flux settings of the laser based on the input geometry parameters.
3. The temperature history is then evaluated to the determine the crystallinity and thermal degradation occurrences. This analysis is carried out by using 'MATLAB R2016a'.
4. This is then compared to measurements done on specimens created by Reichardt[7], and new measurements with the digital scanning calorimetry.

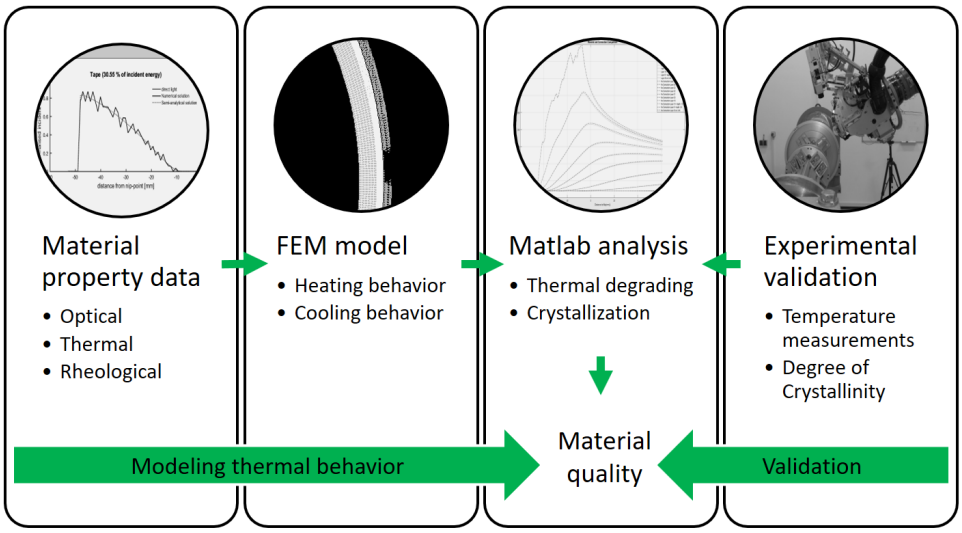

FIGURE 1.8: Methodology schematic

Chapter 2

Thermal Model

This chapter explains the three-dimensional Lagrangian transient thermal model. Section 2.1 explains the choices made for the model, in subsection 2.1.1 are the assumptions of the model, in subsection 2.1.2 the use of the Lagrangian coordinate system is explained, subsection 2.1.3 explains the choice for a transient model instead of a steady state model. The reason for the transition to a complex three-dimensional model is explained in subsection 2.1.4 and 2.1.5. The implemented solution structures are explained in section 2.2 for the simulation of geometry change during tape placement.

The following sections explain settings of the simulation: standard geometry parameters 2.3, boundary conditions 2.4, mesh and step size 2.5 and the FRP that is used in the simulated process 2.6. Section 2.7 explains temperature distribution as described by the three-dimensional energy balance. In section 2.8 is the firstly developed two-dimensional model which was used to test the optical distribution for the heat flux. Using this two-dimensional model it was determined that the role of longitude conductivity in placement direction was insignificant.

The complete three-dimensional model setup is explained in sections: 2.9, 2.10 and 2.11. The three-dimensional simulation model allows for increased complexity in the transverse direction, allowing for multiple studies to be performed with the model using different geomerty's and boundary conditions. In section 2.12 we explain the studies that are performed using the developed model.

2.1 Setup of the Thermal Model

2.1.1 Assumptions

To identify how the material is performing after placement, a new thermal simulation was developed to predict the temperatures during the LATW process. This model is based on the optical results and kinematic model settings for different winding patterns. Grouve[6] already developed a one-dimensional transient thermal model, which is a good starting point in estimating the temperature around nip-point. But with the model developed in this thesis it possible to performer different winding pattern, multiple layers and thus multiple heating and cooling cycles, which also influence the temperature dependent material properties of the substrate[11]. Grouve's[6] model uses the following underlying assumptions:

1. Heating of tape is not influenced by the by the placement, see section 2.3
2. Thermal contact is perfect at all interfaces, such as between tape and substrate after bonding.
3. The process has reached a steady state, with respect to the tape placement head.
4. Effect of radiation is neglected.
5. Roller deformation is neglected.
6. Effect of forced convection is neglected.
7. The effects of in-plane conduction are negligible.
8. Effects of curvature of the tape, roller and substrate may all be ignored.

The last two assumptions 7 and 8 are re-evaluated since literature determined them to be invalid for an accurate temperature history. A further explanation onto why these assumptions are invalid for this model will be discussed shortly in subsection 2.1.3 and 2.1.4 Nonetheless, the rest of the assumptions still hold to adequately perform the simulation.

2.1.2 Lagrangian Coordinate system

The new simulation uses a Lagrangian approach, i.e. with the coordinate system attached to the material. This is a convenient choice since we try to predict material properties of the tape winding model for the whole part and at specific points, a Eulerian model for which the coordinate systems moves with placement would require a more complicated procedure to determine the temperature history at a specific coordinate position. The Lagrangian approach is shown (for the substrate only) in figure 2.1. The roller and laser (boundary conditions) move with a velocity v_{pl} with respect to the substrate, such that this domain before the nip-point experiences a time-varying laser heat flux q(t). The domain at the nip-point has thickness increase or element activation, thus simulating the placement of a new piece of the tape.

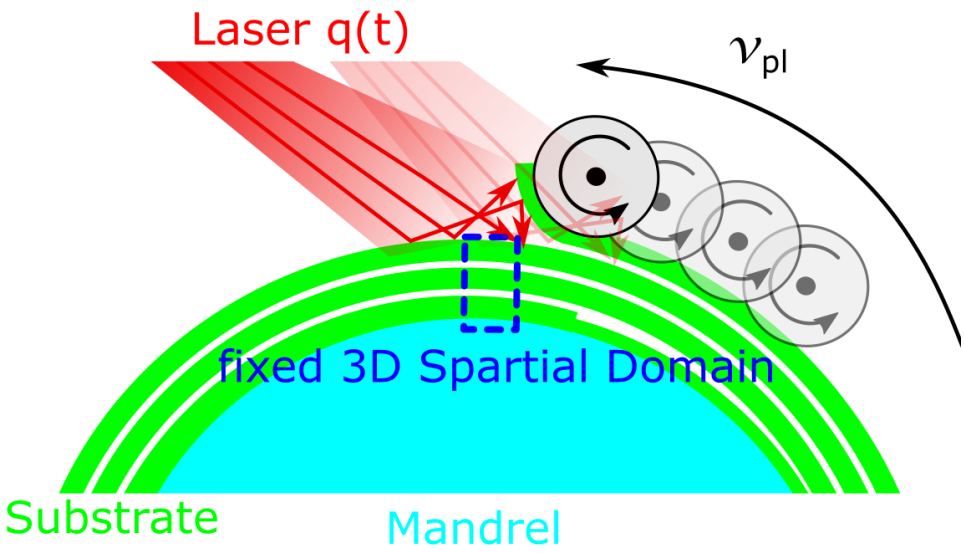

FIGURE 2.1: Lagrangian model

2.1.3 Transient analyses

In a work by Kim[8], there is a comparison between Quasi-Steady state and Transient simulation, see figure 2.2. The quasi-steady state analysis predicts higher temperatures, than full transient analysis. The transient model and its computational implementation were verified using analytical solutions and actual experiments, so in other words, the quasi-steady state analysis was proven to significantly underestimate the heat loss at the composite's outer surface. Further reasons are not explained in the paper, but a transient basis has another advantage as well and that is a time-based geometry. By directly modelling the time-based geometry allows for situations such as hoop winding and adjacent winding to be simulated as well, which can lead to multiple heating and cooling cycles for the substrate. So since the influence of time-based geometry is of importance for this research a transient basis is chosen for the thermal model.

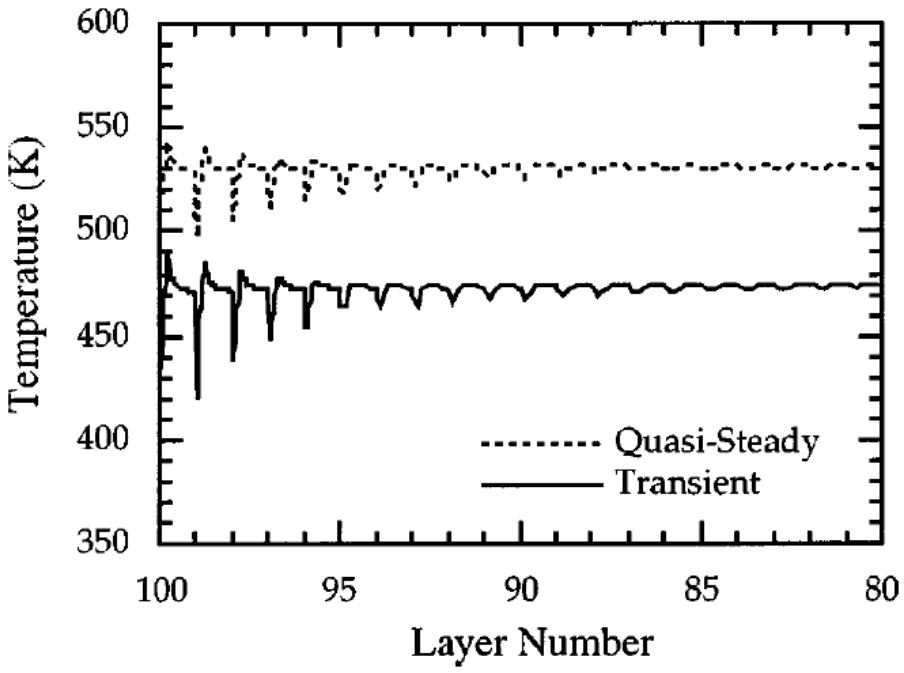

FIGURE 2.2: Comparison of the temperature distributions in the top 20 layers of a composite cylinder wound from AS4/3501-6 prepreg predicted by the fully transient[8] and quasi-steady state[9] approaches. Integer number on the x-axis label represents the layer number. v_{pl}=6.7 mm/s, q = 48.6 kW/m^2.

2.1.4 Two-dimensional model

The thermal model developed by Grouve[6] was a one-dimensional thermal model, using only a one-dimensional model would be ideal since it would not require too much computation time. However research in the FibreChain[11] project determined that neglecting the in-plane conduction, would give a large difference in nip-point temperature, illustrated in figure 2.3.

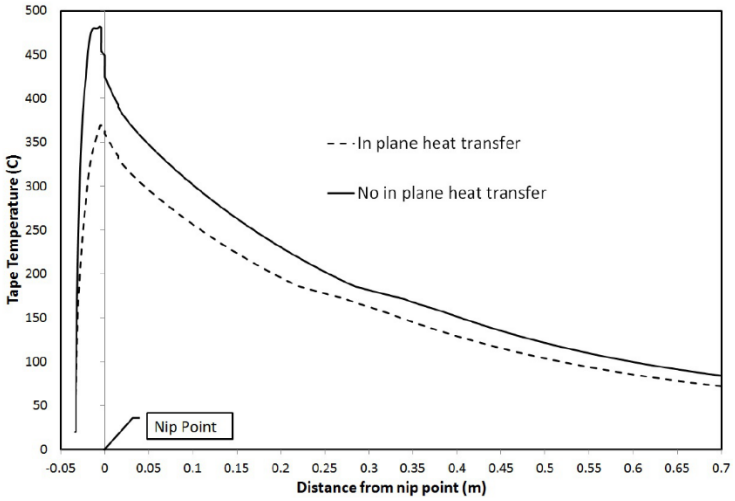

FIGURE 2.3: FibreChain[11], PA12/carbon fibre, Eulerian approach (CFD), v_{pl}=125 mm/s, Power=1500 W.

This research was performed with a Eulerian model, using commercial software of Ansys CFD. The tape placement in this research was simulated using mass flow, and heated with a constant laser power. In this research, it was not determined if this was due to longitude conductivity, transverse conductivity or convection on the side of the tape. The verification of this research leads us to require at least a two-dimensional thermal model, with conductivity in the tape direction since the material conductions coefficient is the highest in the longitude direction.

2.1.5 Three-dimensional model

The problem becomes more complicated for changeable laminate lay-up, see figure 2.4. With a changeable laminate lay-up, it is necessary to go to a three-dimensional thermal model, as well as a complex kinematic model for the creation of the mesh, heating and activation/creation order.

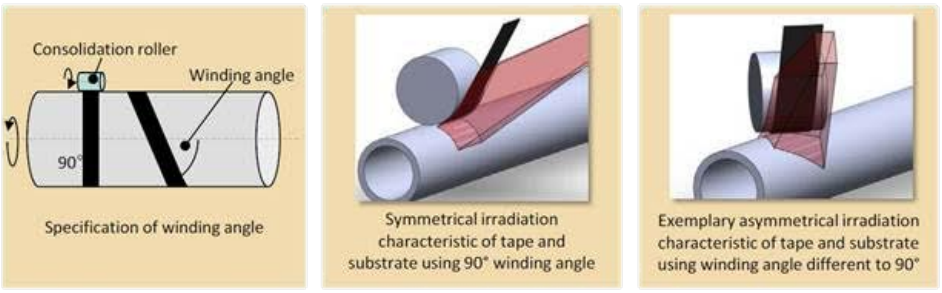

FIGURE 2.4: Angular winding in laser assisted tape winding.

2.2 Solution Structure

Two methods were created to model the three-dimensional behaviour of tape placement in Ansys, the birth-and-death method and the Initial Condition scheme. This was necessary since Ansys does not allow for geometry or element changes during the solution process.

2.2.1 Birth-and-death of Elements

The birth-and-death method uses Solid element and creates the complete mesh in the first step of the solution. It then deactivates elements by putting them into a 'death' state in which it has close to zero conductivity values. The tape layup is then simulated by reactivating 'death' elements with an initial temperature. Ansys sets-up the stiffness/conductivity matrix setup for the complete mesh, but will contain close to zero values for the 'death' elements. When the element is 'birthed' will program change the value in the stiffness/conductivity matrix.

2.2.2 Initial Condition Method

The Initial Condition (IC) method uses three-dimensional Shell elements, these shell elements have nodal equations through-thickness, instead of multiple nodal points. Multiple nodal equations instead of layer thickness reduce the mesh size considerably. This scheme runs the tape placement by performing multiple simulations in a row and changing the mesh at each time step to simulate the tape placement. The temperatures of the previous simulation are implemented as the initial condition for the next simulation.

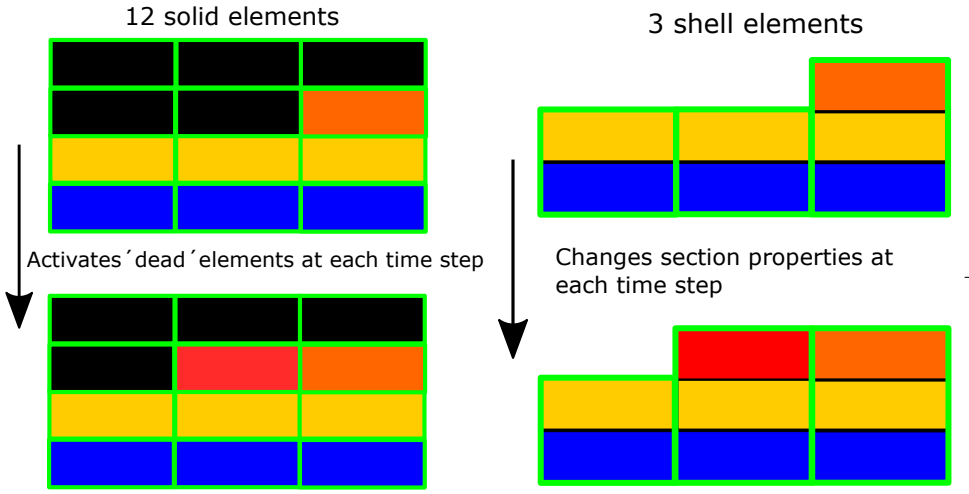

(A) Birth-and-death of Elements

(B) Initial Condition change

FIGURE 2.5: Solution Structures

2.3 Simulation Parameters

Minor parts of Grouve's model are still used, which does not need to be re-evaluated. This is the case for the steady-state thermal data of the incoming tape since the heating of tape is assumed not to be influenced by the placement. Basically, the thermal model by Grouve[6] is used as input data, to provide the steady state initial tape temperature at nip-point for the simulation(can also be done using a measurement at nip-point), so that the heating up of the incoming tape does not have to be modelled.

TABLE 2.1: Global simulation parameters, *=specified value.

Description	Symbol	Value	Unit
Tape			
Tape refractive index[3]	n_t	1.8	
Tape width	w_t	12, *	mm
Tape thickness	t_t	0.15	mm
Incoming tape angle	ϕ_t	-45	°
Tape winding angle	α_t	90,*	°
Substrate			
Substrate refractive index[3]	n_s	1.8	
Substrate width	w_s	36, *	mm
Substrate fibre orientation	α_s	90, *	°
Substrate initial layers	L_0	5,*	
Mandrel			
Mandrel radius	R_s	122, *	mm
Mandrel width	w_s	31.75, *	mm
Roller			
Roller refractive index[3]	n_r	1.4	
Roller y-position (of cylinder axis)	y_r	0	mm
Roller z-position (of cylinder axis)	z_r	35	mm
Roller radius	R_r	35	mm
Roller width	w_r	50	mm
Laserspot			
Laser spot y-position (of centroid)	y_l	-308.61	mm
Laser spot z-position (of centroid)	z_l	111.93	mm
Laser spot height	h_l	28	mm
Laser spot width	w_l	11	mm
Laser beam angle	ϕ_l	-21.73	°
Laser intensity[3]	q	1.461,*	W/mm2
Dispersion unit			
Placement velocity	v_{pl}	100	mm/s

Reichardt[7] added an optical model to Grouve's[6] work which is used to a large extent to compute optical data for the heat flux in the newly developed thermal simulation.

2.3.1 Global simulation parameters

Optical data is first generated using settings of table 2.1 in the previous developed LATW tool[7]. This data is then inputted into the Ansys simulation to compute the required thermal analyses in two-dimensional and three-dimensional. The parameters in table 2.1 are the geometry and laser settings for the optical model and simulation model, these parameters will be used throughout the thesis for all simulations unless otherwise specified.

TABLE 2.2: Boundary conditions

Boundary conditions	Symbol	Value	Unit
Environment temperature	T_∞	25	°C
Initial temperature	T_0	25	°C
Tape Initial temperature at nippoint	T_{t0}	322.87	°C
Tape-air heat transfer coefficient[10]	$h_{t,air}$	10	$W/(m^2C)$
Substrate-air heat transfer coefficient[10]	$h_{s,air}$	10	$W/(m^2C)$
Substrate-air side heat transfer coefficient[10]	$h_{s,side}$	10	$W/(m^2C)$
Substrate-mandrel heat transfer coefficient[10]	$h_{s,mandrel}$	500	$W/(m^2C)$

2.4 Boundary Conditions

Only the substrate was modelled in the thermal domain, whereas the laser heat influx was modelled as boundary conditions. The mandrel was modelled by elements or as convective boundary condition depending on the chosen simulation settings.

The heat transfer around the rotating, heated mandrel is governed by two different mechanisms: natural convection due to the temperature difference between the mandrel surface and ambient air along with and forced convection due to the rotational motion. At the winding speeds used in this study 8–30 rpm, At this velocity, the effect of forced convection is negligible as natural convection dominates the heat transfer.

A large number of studies, such as [8], [12], [13], [14], provide effective heat transfer coefficients between carbon thermoplastic composites in contact with aluminium tooling $h_{s,mandrel}$ and air convection $h_{s,air}$. The values mentioned in these studies for the composite-aluminium mould contact $h_{s,mandrel}$ vary between 400 and 1000 $W/(m^2C)$, while the convection coefficient for air h_{air} is approximately 10 $W/(m^2C)$ in most cases. The present analysis neglects thermal effects caused by the roller such as heat loss through conduction to the roller since the roller is made of an elastomer with negligible conductivity compared with the conductivity to the mandrel and also since an elastomer heats up to a temperature comparable to that of the substrate.

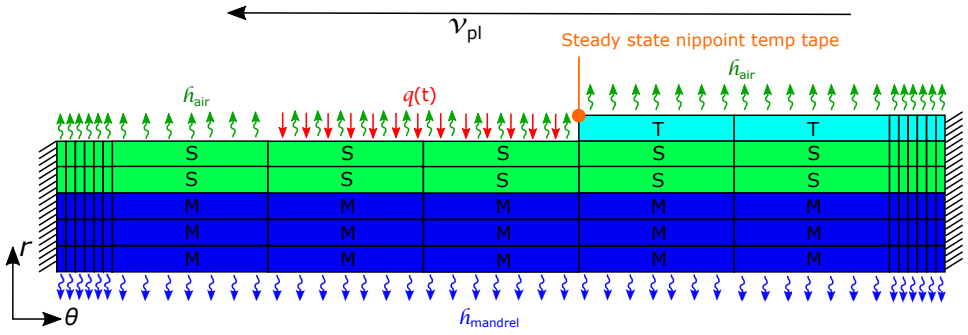

FIGURE 2.6: Boundary Conditions

TABLE 2.3: Mesh Simulation Parameters

Simulation Parameters	Symbol	Value	Unit
StepSize	Δt	0.01	s
MeshSize	M_s	$l_e \cdot w_e$	mm^2
Areafactor	A_f	1.8	
Areafactorbefore	$A_{f,before}$	0.6	
LayUpsubsteps	S_L	5	
Timeskipsubsteps	S_t	20	
Mesh Parameters			
globalelementswidth	w_e	$w_t/10$	mm
globalelementslength	l_e	1	mm
Meshrefinement	M_r	0	

2.5 Mesh and Step Parameters

One of the relevant parameters is to determine the mesh size and time step size, the used time step and mesh size are of 0.01 second and 1mm in length respectively. This was determined by a matter of convergence of the solution with an accuracy of 2%. Further refinement can be done to increase the mesh size by adjusting the mesh refinement parameter to a higher value, which quadratically increases the mesh size, see table 2.3 for all parameters.

2.6 Material Properties

The fibre-reinforced polymer used throughout the thesis is AS4/PEEK with a 61% fibre volume fraction, this material is chosen since it is widely studied, and the necessary material data sheets[12] are available for temperature depended material behaviour as well as information on the crystallinity growth. Composite materials have at least two constituents: reinforcement and matrix. The reinforcement material is the carbon fibres, which add strength in longitude direction, while the matrix keeps the fibres in place and transfers the load applied to the fibres. The focus of this research is the polymer matrix system (see figure 2.7), since the matrix material is re-melted, while the carbon fibres remain intact.

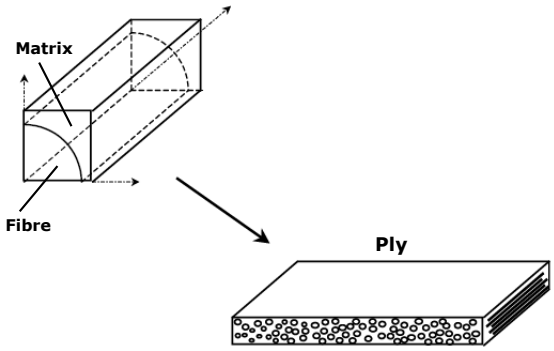

FIGURE 2.7: Fibre-matrix scale, ply scale

2.6.1 Polymer Matrix System

The matrix material Poly-Ether-Ether-Ketone (PEEK) is a high-performance semi-crystalline thermoplastic. It is considered a low crystalline polymer since its maximum crystallinity is close to 40%[15]. The glass transition temperature T_g of PEEK is 143 °C[16] and the melting temperature T_m is around 343°C[17]. The onset of thermal degradation resulting in mass loss occurs between 575 and 580°C[18].

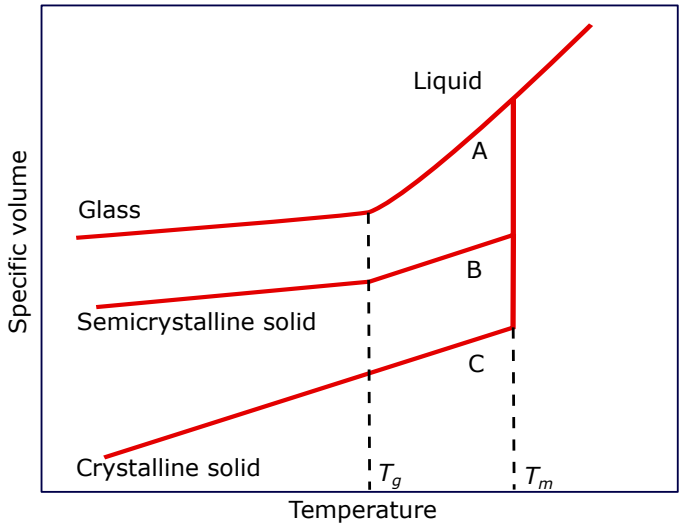

FIGURE 2.8: Phase Diagram of Polymer and Glass material

2.6.2 Degradation and decomposition

Material degradation is first followed by decomposition, in the first decomposition step, random chain scissions of the ether and ketone bonds of figure 2.9 is believed to be the main mechanism[19], this pyrolysis starts at a temperature of 450°C, a second and third decomposition occurs at respectively 650°C and 750°C, but at just under 600°C does the thermal degradation begin which results in a rapid and significant mass loss. The volatilisation is around 20% of the polymer mass for a carbon-peek composite, of which the remaining polymer mass appears to be carbonaceous char[20]. Taking the first step of decomposition of the polymer into account is beyond the scope of the work, so we will only look at the occurrence of thermal degradation of the composite during LATW.

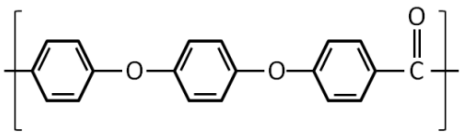

FIGURE 2.9: Mer units of Poly-Ether-Ether-Ketone.

TABLE 2.4: Temperature dependent material properties[12]

Temperature $^\circ$	Specific heat $J/(kg^\circ C)$	Density Kg/m^3	Conductivity (axial) $W/(m^\circ C)$	Conductivity (transverse) $W/(m^\circ C)$
Independent of T	1425	1560	5	0.72
0	800	1601	3.5	0.42
50	930	1598	4.6	0.52
100	1040	1593	5.1	0.6
150	1260	1586	5.9	0.7
200	1300	1575	5.9	0.7
250	1400	1563	6.1	0.7
300	1550	1551	6.7	0.75
350	1650	1537	6.8	0.68
400	1700	1524	7.0	0.65

2.6.3 Temperature depended material

In previous research[7] fixed material values were used to determine the temperatures during LATW, with the new three-dimensional simulation model it is possible to use temperature dependent material behaviour for the thermal model, see table 2.4.

To determine the effect of temperature dependent material on the temperatures during Laser Assisted Tape Winding, we used the three-dimensional simulation model of section 2.9. With the KOT model, it is possible to use temperate dependent material behaviour. Thus we compared the fixed material properties to the temperature dependent properties, see table 2.4. The results determined the critical material parameters and the changes it has on the temperature history during LATW. This study is done in appendix E, which showed that temperature depended through-thickness conductivity results in a lower heating temperature by the laser $20 \circ C$, but has a slower cooling rate for temperatures below $150 \circ C$. Temperature depended heat capacity resulted in faster heating and cooling rates, which were excepted given that the constant value is higher for almost all occurring temperatures, and rest of temperature depended material value had less $1 \circ C$ difference compared to the constant values.

2.7 Energy Balance

2.7.1 One-dimensional thermal problem

The thermal problem is governed by of the heat flux, convection and the conductivity. In one-dimensional calculations, only through thickness(z-direction) conductivity and convection with the Lagrangian approach was adopted to describe the thermal problem, which gives temperature distribution as described by the one-dimensional energy balance[21]:

$$\rho c_p \frac{\partial T}{\partial t} = k_z \frac{\partial^2 T}{\partial z^2} \tag{2.1}$$

With ρ the density, c_p the specific heat, $T = T(z,t)$ the temperature, t is time and k_z the through-thickness thermal conductivity.

2.7.2 Three-dimensional thermal problem

The three-dimensional formula is described by the Mechanical APDL Theory Reference[22] for the thermal distribution. In which the first law of thermodynamics is specialised to the differential control volume, and Fourier's law is used to relate the heat flux vector $\{q\}$ to the thermal gradients of the conductivity matrix $[D]$. This gives us the following formula for the three-dimensional thermal problem:

$$\rho c_p(\frac{\partial T}{\partial t} + v^T\{L\}T) = \{L\}^T[D]\{L\}T + \ddot{q} \tag{2.2}$$

Here the temperature is function of time and space: T = T(x,y,z,t)

{v} = the velocity vector for mass transport of heat,

$\ddot{q}$ = the heat generation rate per unit volume,

{L}= $\begin{bmatrix} \frac{\partial}{\partial x} & \frac{\partial}{\partial y} & \frac{\partial}{\partial z} \end{bmatrix}^T$ is the vector operator,

$[D] = \begin{bmatrix} K_{xx} & 0 & 0 \\ 0 & K_{yy} & 0 \\ 0 & 0 & K_{zz} \end{bmatrix}$ is the conductivity matrix.

With the Lagrangian approach, there is no {v} mass transportation and with the assumption of no chemical reactions, we can ignore the $\ddot{q}$ the heat generation rate per unit volume. Writing out the matrix computation we then get the formula for the three-dimensional thermal distribution in the global Cartesian system:

$$\rho c_p \frac{\partial T}{\partial t} = \frac{\partial}{\partial x}(K_x x \frac{\partial T}{\partial x}) + \frac{\partial}{\partial y}(K_y y \frac{\partial T}{\partial y}) + \frac{\partial}{\partial z}(K_z z \frac{\partial T}{\partial z}) \tag{2.3}$$

The fundamental boundary condition in the system gives rise to equations for the heat flux and convection. The imposed boundary conditions are presumed to cover the entire element. In Ansys it is specified that the convection or heat flux surface act over the full surface of the element, and use Newton's law of cooling:

$$\{q\}^T\{\eta\} = -h_f(T_S - T_B) \tag{2.4}$$

With $\{\eta\}$ = unit outward normal vector, T_B=bulk temperature of the adjacent fluid and T_S=temperature at the surface of the model. Where: h_f = film coefficient this is evaluated at $(T_B + T_S)/2$ unless otherwise specified for the element, for example with heat flux, then it's a value of 1.

Unfortunately, they are both governed by the same surface equation, a problem arises when applying both convection and heat flux on the same surface. To solve this problem an extra surface element was modelled on top of the existing element especially for the heat flux, this gives rise to surface E at the top.

$$\{\eta\}^T[D]\{L\}T = -h_f(T_S - T_B) \tag{2.5}$$

Premultiplying EQ 2.2 by a virtual change in temperature, integrating over the volume of the element, and combining with EQ 2.4 and EQ 2.5 with some manipulation yields the three-dimensional-dimensional energy balance for a single element:

$$\int_V (\rho c_p \delta T \frac{\partial T}{\partial t} + \{L\}^T(\delta T)\{L\}T)d(V) = \oint_S \delta T \cdot h_{conv}(T_B - T)d(S) + \oint_E \delta T\{q\}d(E) \tag{2.6}$$

with: V= volume of the element and δT= an allowable virtual temperature $(= \delta T(x, y, z, t))$.

2.8 Optical-Thermal Model

First, a transient two-dimensional optical-thermal model was developed, to test the two-dimensional effects and the optical distribution with the Ansys. With the LATWtool [7] an optical distribution was created for the global settings in table 2.1. The optical distribution was imported into the thermal model as settings for the heat flux of the laser. The two-dimensional optical-thermal model used the birth-and-death method, with Plane elements to simulate tape placement for multiple full windings.

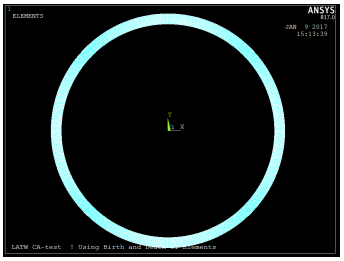

FIGURE 2.10: Two-dimensional Simulation Model

2.8.1 Effect of conduction in winding direction

The transient two-dimensional optical-thermal model is simulated using the global settings table 2.1 and was compared to the same model with 'almost' negligible longitude conduction, see figure 2.11. The difference is shown in figure 2.11 is almost indistinguishable and not comparable to what is seen in figure 2.3 of the Fibrechain research [11]. One of the conclusions we could draw from this model was that the influence of longitude conductivity was almost negligible, therefore further development was necessary to explain the in-plane effects described in section 2.1.4. The three-dimensional model was thus further concluded to be necessary to examine in-plane effects of transverse conductivity, side convection and substrate/mandrel conduction.

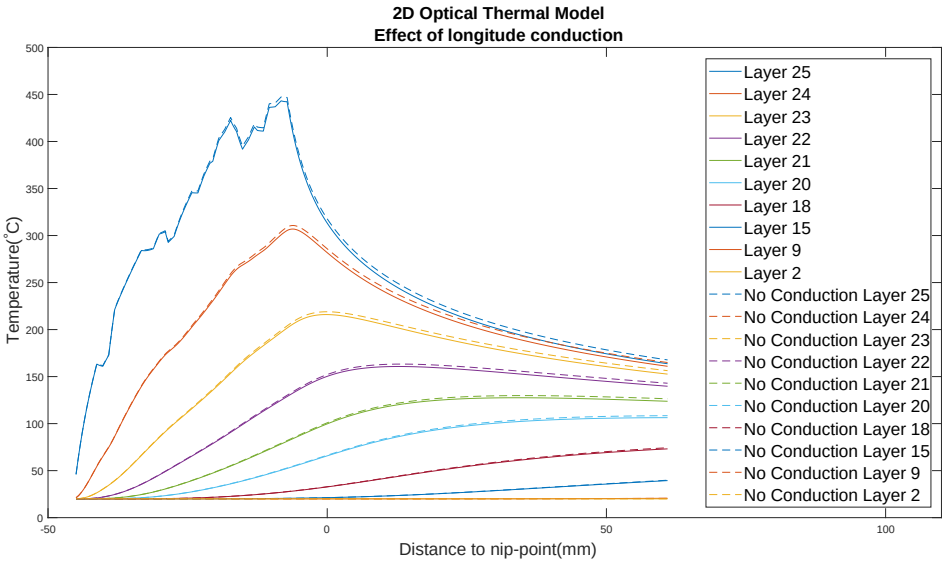

FIGURE 2.11: Two-dimensional simulation of a single placement, with and without longitude conductivity on a 25 layer substrate

2.9 Kinematic-Optical-Thermal Model

The three-dimensional simulation model is more complicated than the two-dimensional simulation model in the method, elements and solution settings. The KOT model uses 3-D layered SHELL131 elements having in-plane and through-thickness thermal conduction capability. Shell elements consist of a single element in the thickness direction, instead of having multiple volume elements in the radius/thickness direction. This leads to decreases in complexity by geometry in the thickness direction, since it allows for the positions through thickness being described by a single node. Thus decreases the computational time of the scheme. This was verified by the outcome of a comparison was between the method with 3D volume elements using the birth-and-death method (similar to the two-dimensional model) and the 3D shell element with initial conditions method (refer to Appendix A for the method and element comparison). As in the two-dimensional Model, the 3D model also uses a Lagrangian reference frame, with a polar coordinate system.

The IC simulation method works by performing multiple simulations in a row and copying the temperature distribution as the new initial conditions for the next time step. At the start of the next simulation, it changes the section properties of the element to simulate a single element of tape placement, see figure 2.12b. The next simulation also inputs all temperature of the previous simulation as the initial temperatures and sets the boundary conditions to the corresponding position, this process is repeated for all time steps. At the end of each simulation are the temperatures compiled in a database for the complete thermal history at specific points.

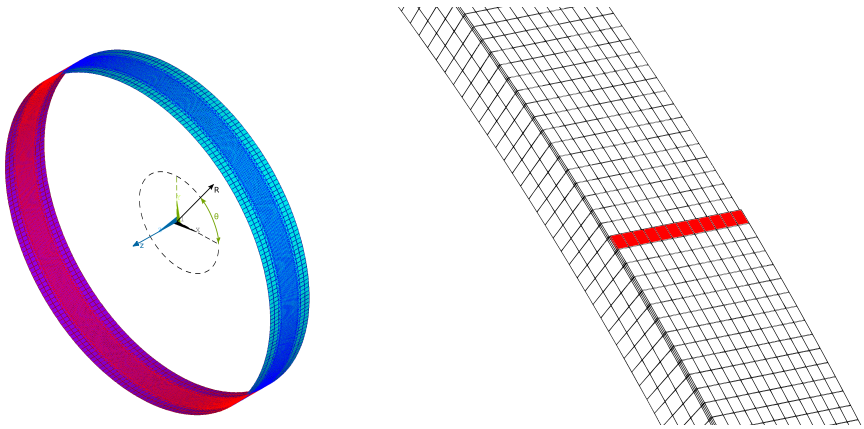

(A) Polar coordinate system (B) Changed section elements

FIGURE 2.12: Kinematic-Optical-Themal simulation settings

2.10 Simulation Setup

The simulation consists of four parts: the first part is the implantation of the simulation settings, second the creation/addition of the material, third the computational part of the process simulation and fourth part the data collection for the complete thermal history at specific points for further analyses. A complete overview of the simulation setup is shown in figure 2.15.

2.10.1 Simulation Settings

The simulation starts with the implementation of the user settings, the creation of the mesh and boundary conditions. The creation of the mesh is based on the settings for the geometry and layer built-up. Shell elements are bit harder to connect to one another when they have different section properties, see figure C.1 This is solved by using constraint equations to couple the two elements.
To apply the constraint equation an additional node is necessary. Otherwise, the top temperature/'TTOP' C.1b is poorly matched. Normally, both layers should be matched, i.e. layer 2 matched to layer 2. By created an additional node for the second element, the standard method for matching elements can be evaded. A constraint equation equalizes the nodal values of the two elements to their corresponding layer, as seen in C.1c.

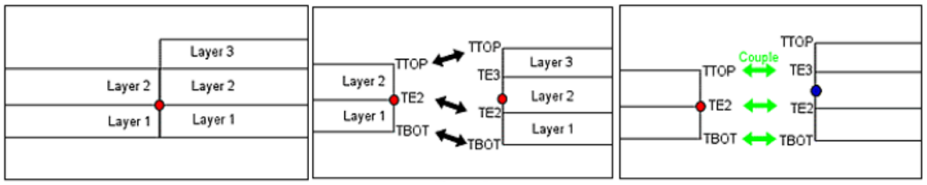

(A) Shared node (B) Standard coupling (C) Adjusted coupling

FIGURE 2.13: Coupling of SHELL131 elements[23]

2.10.2 Process Simulation

In short, the computational extensive part of the simulation is consecutively solving for the placement of a small 1mm piece of tape. The following illustration 2.14 and description will explain terminology between a hoop windings and adjacent windings in the simulation process

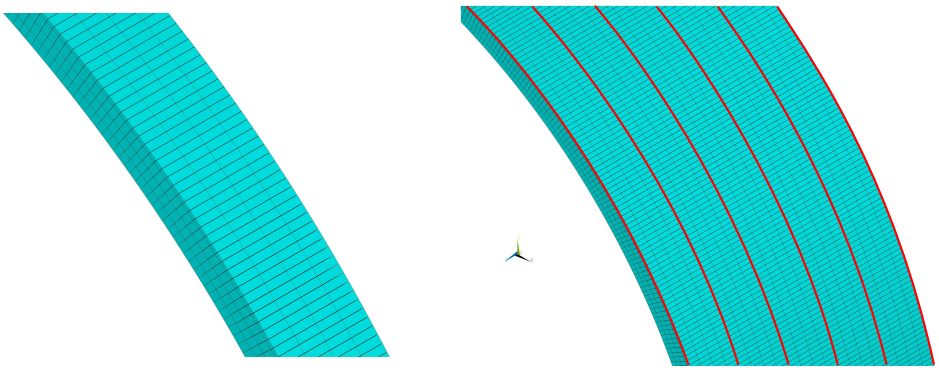

(A) one hoop winding

(B) five adjacent windings

FIGURE 2.14: Terminology difference between windings and layers in KOT model.

2.14a After 1mm piece of tape has been wound, boundary conditions are adjusted and the system will be solved. The results of this simulation will be implemented as an initial condition in the next simulation. This progress is repeated for all time steps to place one hoop winding, and for every layer, a hoop winding is performed.

2.14b In the case of adjacent windings, the winding is repeated for multiple hoop winding, with the only difference being that the tape is placed next to the initial winding. This then repeated for multiple layers starting from the initial winding position.

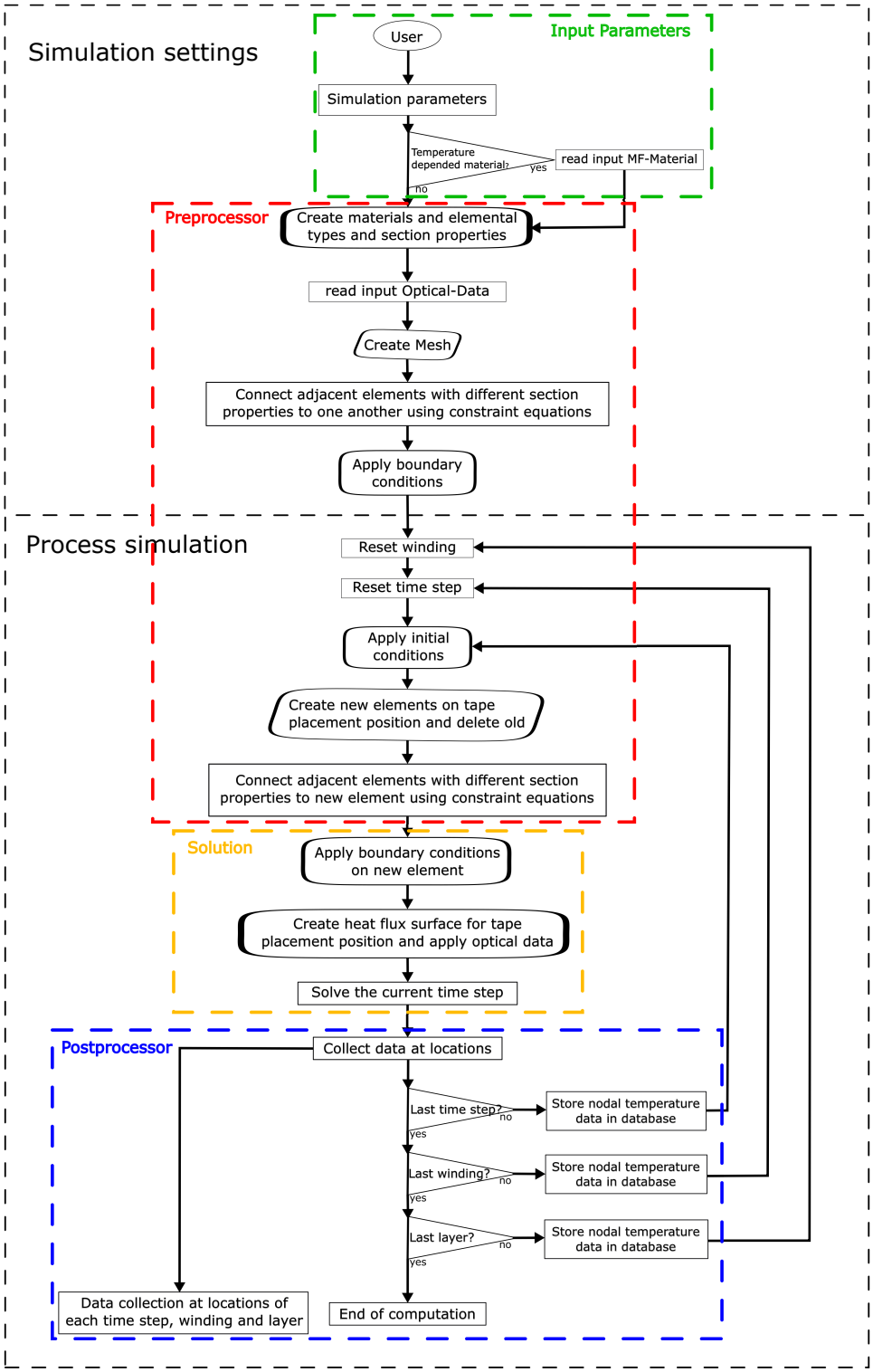

FIGURE 2.15: KOT model simulation schematic

2.11 Model Reduction

With all the additional steps, the model has become time-consuming, sometimes running up to a whole week. To reduce simulation time a few reductions were made to KOT model.

The most fundamental reduction is going from full circular winding to only wind the first 240mm of the perimeter, see figure 2.16. To still complete the 360° winding, a time delay was calculated based on the removed perimeter, see equation 2.7.

$$t_{delay} = dt * ((2 * r_m * pi * 1000) - (A_f * v_{pl} * 1000)) \tag{2.7}$$

A study validating this reduction of the model size was performed in appendix D. This study was performed by calculating the nip-point temperature and thermal history of the full and reduced model for three adjacent windings with each three layers. The study confirms that the nip-point temperatures and temperature history agree with one another for the full and reduced perimeter.

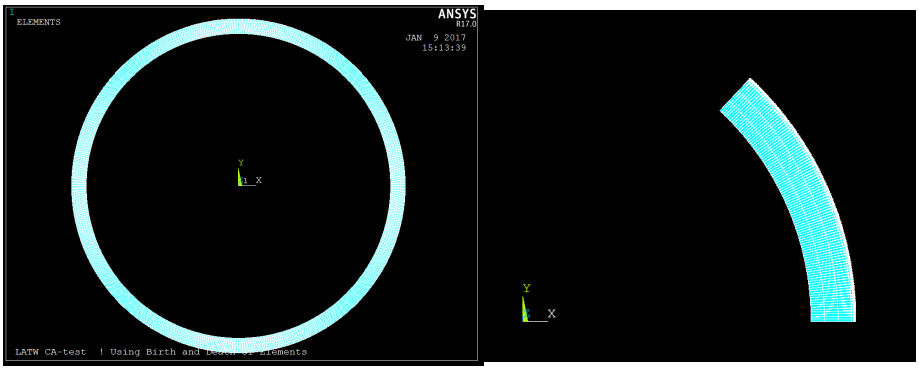

(A) Full Model (B) Reduced Model

FIGURE 2.16: Model size reduction

Another significant reduction was also made by cutting the model vertically in half, with symmetric condition. This can only be applied when there are no adjacent windings, a 90° tape winding angle and with 0° or 90° substrate fibre orientation angle for all layers.

2.12 Simulation Options

The new 3D KOT model allows for a large variety of options to simulate the LATW process, including variation in tape width, radius, layer build up, multiple windings, temperature depended material, optical data implementation, transverse conductivity, mandrel material and convections.

2.12.1 Model case study

The simulation model allows multiple settings regarding transverse effects. One of the research questions was the **investigation of change in temperature history, as a result of transverse boundary conditions in width direction**, this is studied by reducing the transverse complexity of the simulation model to its bare essentials in order to determine the geometry and boundary conditions that affect the material quality, see figure 2.17. Another of the reasons to study this is that although the reduction gives a loss of data, it also decreases the simulation time.

The reduction of transverse conditions leads to multiple geometries to be studied, each of the models of 2.17 is compared to one another in chapter 5.

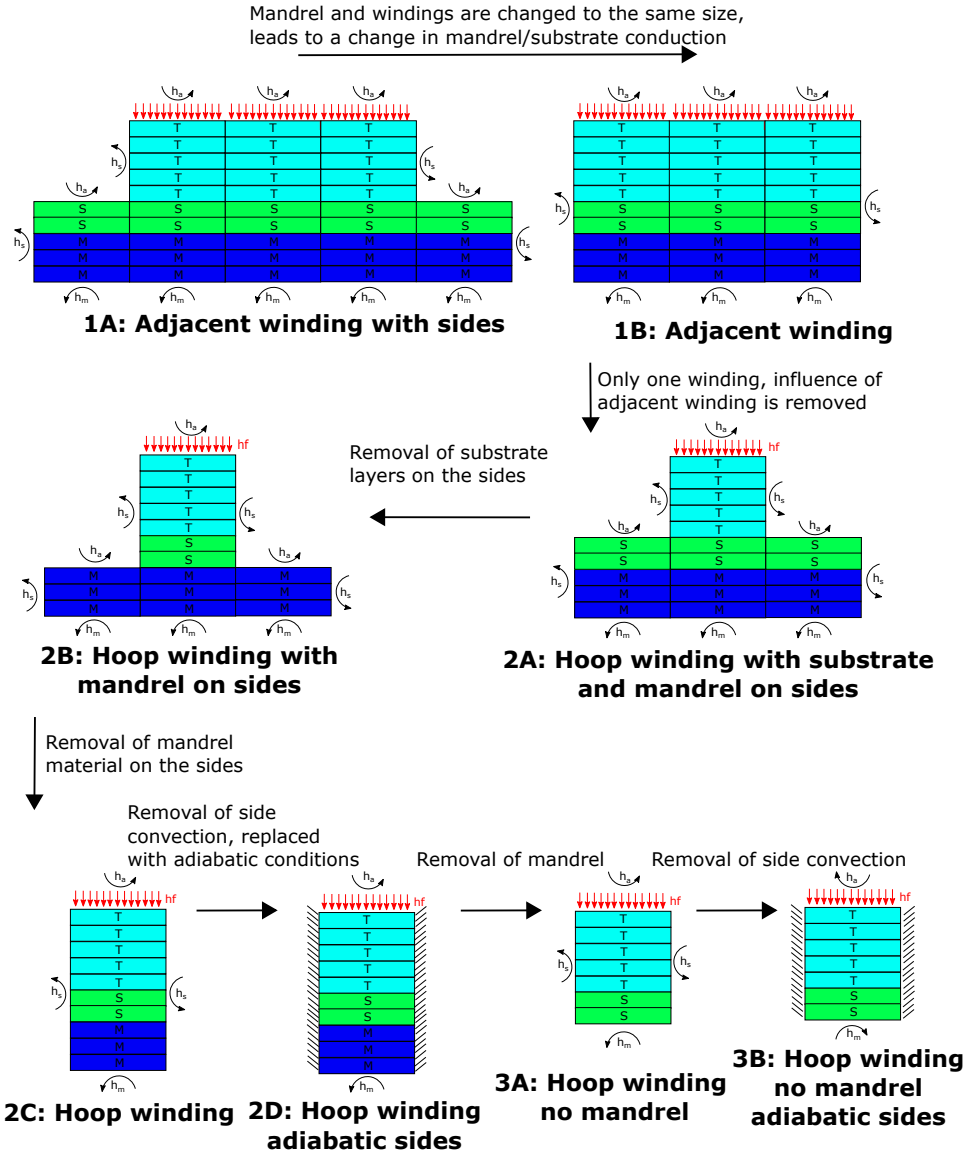

FIGURE 2.17: Model case study's, by reducing the KOT simulation complexity

2.12.2 Variation in tape width and radius

In the tape winding simulation, the influence of geometry parameters has a large effect on the outcome of the material properties. By variating these geometry parameters we can determine the effect on temperature development during the simulation. Different widths of tape are commercially available ranging from 6mm up 300 mm, so being able to consider the effect of tape width could have an influence on the design aspect. Complex geometry normally variates a lot in radius, so for tape winding, it is interesting to learn the effect of tape radius using the three-dimensional simulation.

2.12.3 Lay-up build up

To investigate **the consequences of lay-up on the heating and cooling cycle** stacking sequence of the tape winding on 0°, 45° and 90° fibre-orientated substrate is considered, for four positions in tape width direction: at the edge, 2mm of the edge, 4mm of the edge and at the centre. This is important since during production it could determine the laser setting, depending on substrate fibre-orientation and substrate thickness.

2.12.4 Adjacent windings

One of the advantages of three-dimensional simulation for tape winding is to be able to determine the transverse influences of the substrate next to the tape. In a conventional two-dimensional model this influence is neglected, but depending on the laser setting the adjusted tape can reach a temperature above T_g, which changes the material properties of the substrate, or with consecutive windings can the heat of the adjacent layer influence the thermal history of the next winding.

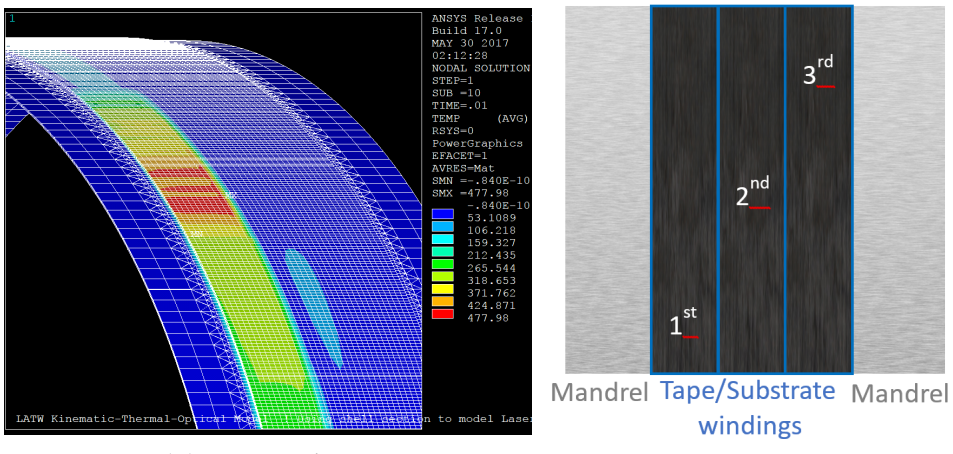

(A) KOT simulation

(B) Winding patron

FIGURE 2.18: Adjacent windings

2.12.5 Mandrel Material

The conductivity of the mandrel has a large effect on the simulation. In practice, it is of interest to wind on top of different materials. In this study, we examine the difference between winding on a steel, aluminium and PEEK. Especially the thermoplastic material is of interest since this will have a melted bond with the Carbon-PEEK tape.

2.12.6 Environment Temperature

The manufacturing environment temperature has a larger influence on LATW process since all heat is dissipated through conduction to the tooling and convection to air. This rate of heat dissipation has an effect on the crystallinity, therefore the change of the initial temperature and environmental temperature is researched for the temperatures of 25°C, 35°C, 45°C, 55°C and 65°C.

Chapter 3

Crystallinity Model

Crystallization growth occurs during and after tape winding, a model was created to predict the growth during the multiple heating and cooling cycles based on the cooling rate and enthalpy activity. Crystallinity prediction for a constant cooling rate is compiled and fitted in section 3.2. This method is deemed invalid for LATW in section 3.3, in which is shown that the heating and cooling rate changes significantly with temperature and consists of multiple cycles. To determine the crystallinity growth related to temperature, was in section 3.4 the peak crystallisation times compiled and fitted. The peak crystallisation times were converted to percentage based activity, for the temperatures between T_g and T_m. The crystallinity model in section 3.5 calculates the cooling and heating rates for all time steps from the temperature history. From the rates it calculates the crystallinity based on the constant cooling rates of section 3.2 multiplied by the percentage based activity of section 3.4, the sum is then taken to get the crystallisation growth of per cycle.

3.1 Crystallinity

Polymers typically consist out of amorphous areas and crystalline areas, where the percentage of crystalline areas is called the crystallinity. When the polymer is melted, it solely consists out of amorphous areas. The amorphous areas of the polymer can crystallize upon cooling from melt temperature (T_m), by mechanical stretching or via solvent evaporation. The crystallization of polymers is a process related to the partial alignment of molecular chains. The molecular chains fold together and form ordered regions called lamellae, which compose larger spheroidal structures named spherulites[24]. The degree of crystallization affects optical, mechanical, thermal and chemical properties of the polymer.

The crystallinity can be estimated by different analytical methods, such as Different Scanning Calorimetry(DSC), X-ray diffraction, Density measurements, Infrared spectroscopy (IR) and Nuclear magnetic resonance (NMR). In this research, we used the 'Mettler Toledo' DSC to measure the crystallinity of our specimens.

The nucleation density and spherulitic growth rates of the different polymorphs of polymers are, in general, difficult to measure in a single experiment, especially when high cooling rates and/or elevated pressures are required to induce a specific crystal phase. Therefore, crystallization kinetics of the different polymorphs are not well established as a function of temperature and pressure.[25] The matrix material PEEK fits in well with the generally accepted picture for a semi-crystalline polymer. Experimental measurements show that PEEK is a two-phase crystal/amorphous structure consisting of crystalline lamellae, whose thickness increases with crystallization temperature[26].

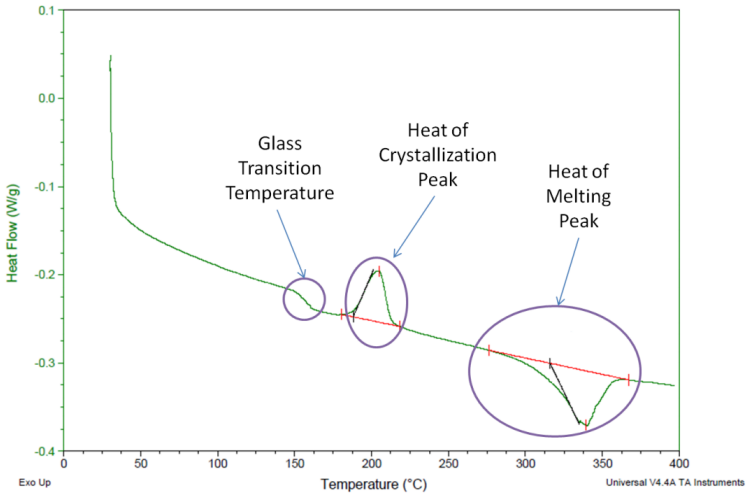

FIGURE 3.1: Typical DSC chart of heat flow with respect to temperature.

3.2 Crystallinity based on Cooling Rate

The crystallinity growth of AS4/PEEK has been researched with different cooling rates and has been compiled by Gao[27] and reproduced in figure 3.2. The cooling rate is plotted on a logarithmic scale plotted on the x-axis and the crystallinity percentage on the y-axis. From this data collection, a logarithmic fit was made to determine crystallinity for all cooling rates. With a linear temperature loss from melt to glass transition, it is possible to determine the crystallinity of AS4/PEEK based on this graph.

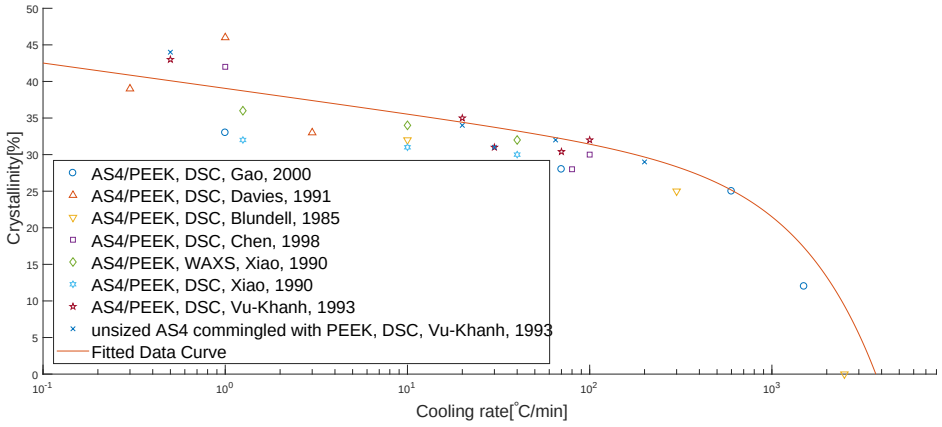

FIGURE 3.2: Degree of crystallinity as a function of cooling rate for carbon fibre/PEEK composites.

Unfortunately the cooling rate in LATW is more complex with a nonlinear curve and multiple reheating's with temperatures up to or below melt, see figure 4.3.

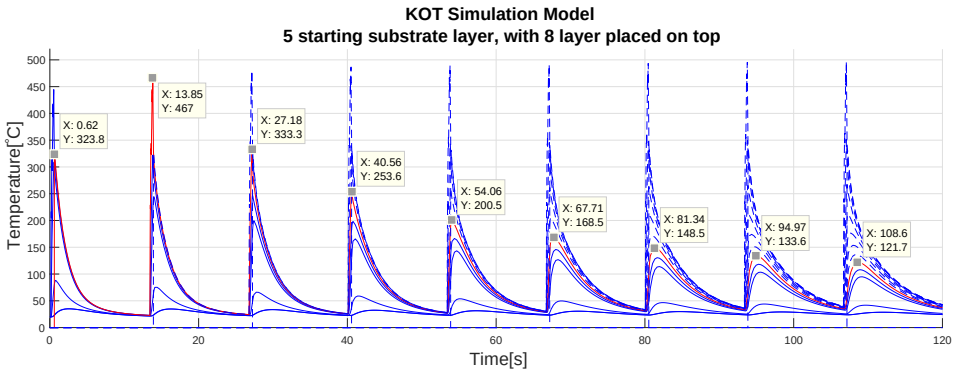

FIGURE 3.3: Temperature history curve of the 6th layer(red) with 9 hoop layers, KOT model, hoop windings: 2C

3.3 Cooling rate in LATW

The simulation, as well as experiments, show multiple heating's of the material with each layer placement, see figure 3.3. The illustration shows the thermal history of the temperature curve of the 6th layer (redline), with another 8 layers being placed on top it. Important to note: not only does the first placement affect the material properties, the hoop windings also influence the material. This occurs since the heating by the hoop winding influences the lower layers to temperatures above T_g and even to temperatures above T_m(normally only the case at the first hoop winding since melting temperature is required for a sold bonding between layers).

The first heating peak is due to the placement of the tape, the second peak is bonding with the next layer, then hoop heating peaks occur from the winding of the next layer above the 6th layer. Only after the placement of the 12th layer, does the 6th layer no longer reaches temperatures above T_g.

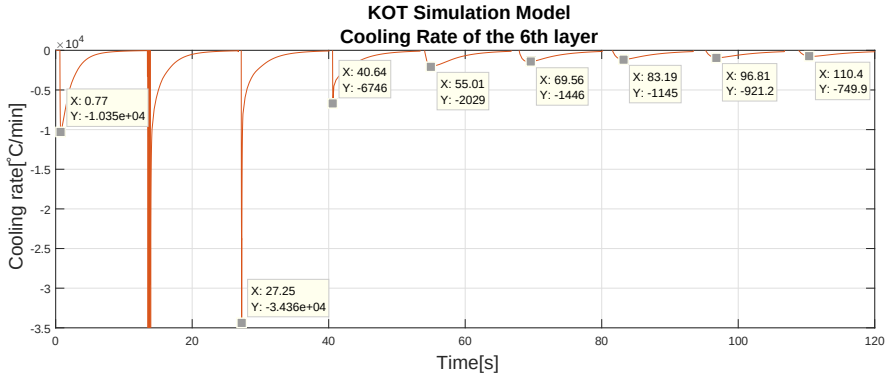

FIGURE 3.4: Cooling rate curve of the thermal history in figure 3.3

Figure 3.4 shows the derivative in time of the temperature curve of the 6th layer, or in other words the cooling rate curve. No crystallinity will appear at a cooling rate above 3250°C/min. However, when consecutive tapes are wound on top of this tape, it will undergo another heating-cooling cycle which will be less intense compared to the first cycle. But if these cycles are within the temperature range where most crystals are formed(above T_g and below T_m), then each cycle results in a different crystal growth. It is therefore important to trace the complete heating/cooling cycles, but also take the temperature into account.

3.4 Crystallinity based on phase transition

To take into account the rate of crystallinity forming, we look at the enthalpy activity. Crystallization can occur over the whole temperature range, normally during cooling yet it can also occur at a fixed temperature(between T_g and T_m).

One of the methods to describe the change of matter from one state to another at a constant temperature is the Avrami equation. The Avrami equation describes the ratio of the crystalline phase $\alpha(t)$, with respect to time t. With the Avrami kinetic coefficient K_{Av} and Avrami exponent n determined experimentally by measuring the different crystallization growth rates at a constant temperature.

$$\alpha(t) = 1 - exp(-K_{Av} \cdot t^n) \tag{3.1}$$

The Avrami kinetic coefficient has been evaluated from isothermal crystallization in the range between 143°C and 310°C, by Tardif[28], Kuo[29], Wang[30] and their respective colleagues for the matrix material PEEK. Using the Avrami equation, the data of the evolution of the crystallization enthalpy has been compiled in figure 3.5.

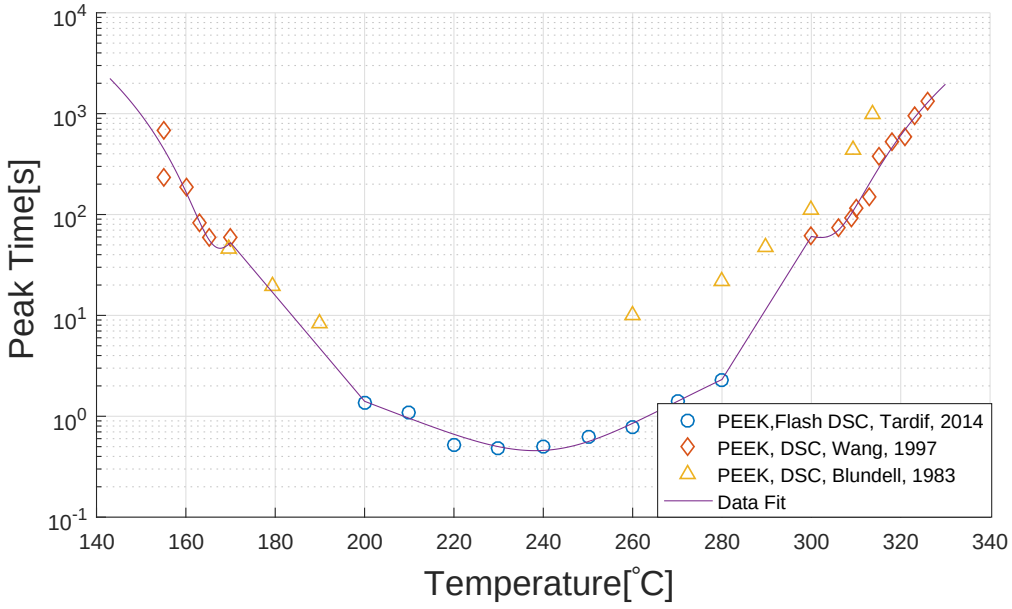

FIGURE 3.5: Peak crystallisation times of PEEK for temperatures between T_g and T_m.

The peak crystallization times in figure 3.5 determines the rate of crystallisation at a specific temperature. Above and below the interval of 200-280°C, the crystallization peak times increases quite quickly as the crystallization is more and more controlled either by diffusion at low temperatures or by nucleation at high temperatures[28].

By creating a data fit we can form a curve for the entire scope between T_g and T_m. The fitted data for crystallisation times were converted to percentage based activity, for the temperatures between T_g and T_m. The percentage-based activity is then multiplied by the crystallinity growth of every cooling rate. This is done so that the crystallinity growth occurs at temperatures with quicker peak crystallisation times, by doing so it makes the growth temperature depended.

3.5 Crystallinity based on Cooling rate and Enthalpy

The crystallinity model is the combination of the crystallinity by constant cooling rates of section 3.2 multiplied by the temperature based percentage activity of section 3.4. The crystallinity model first calculates the cooling and heating rates for all time steps from the temperature history created by the KOT simulation model. From the rates it calculates the crystallinity growth of each time step for the temperatures between T_g and T_m, all these crystallinity growths are then multiplied by percentage activity corresponding to the temperature of that time step and divided by a timestepfactor for the size of the time step, to get the specific crystallinity growth of that time step. The sum is then taken of all specific crystallinity growths values, to get the total crystallinity growth of the thermal history. This timestepfactor was calculated so that the size of the time step does not influence the amount of crystallinity growth. The model was set up so that for constant cooling rates still has the same crystallinity growth occurs in figure 3.2.

The crystallinity model makes two assumptions, which are:
- Time has no influence on the crystallisation growth rate.
- The crystallinity present does not affect the growth rate.

These assumptions can be made since the crystallisation growth that occurs during the LATW process is less than 10%, thus has not reached the peak/half-time crystallisation times. In this study it is also not necessary to accurately predict the crystallinity beforehand in extreme isolation: it suffices to look at the resulting effect of different simulation settings on the crystallinity. The behavioural result on the crystallinity of different settings is more vital in this research than pinpointing the exact percentage of the different crystallinity growths, which is beyond the scope of this study.

Compiling the two graphs of figure 3.2 and 3.5 results in the 3D surface depicted in figure 3.6, for which the crystallinity is the sum of all occurring data point of thermal history.

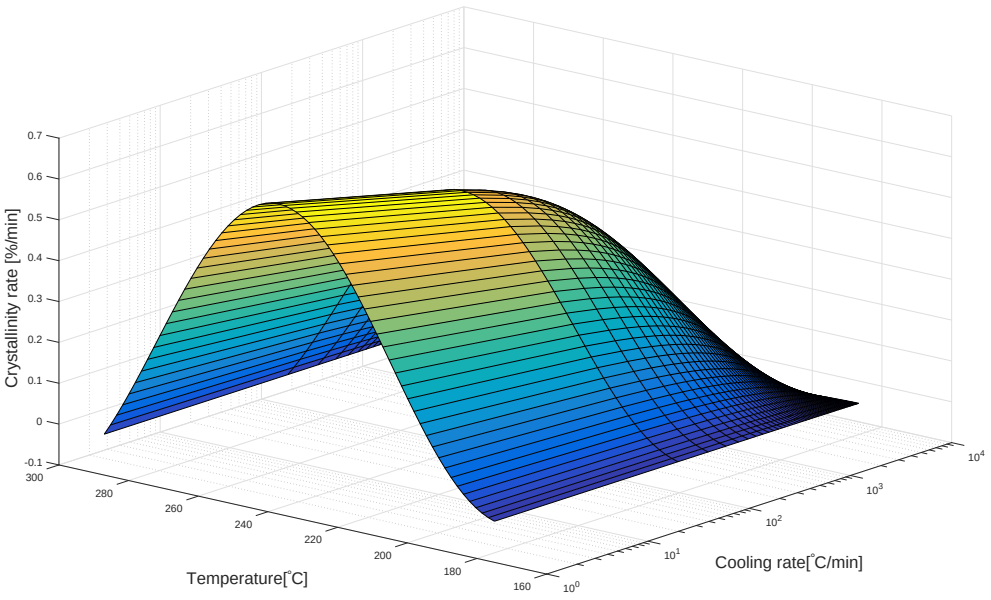

FIGURE 3.6: Crystallisation rate of Carbon-PEEK.

Chapter 4

Experiments

Reichardt[7] created two Carbon-PEEK rings and collected thermocouple data during the production, these specimens are further examined in this chapter. See section 4.1 for information on the specimens and the creation process. In section 4.2 post process thermocouple measurements are analysed and compared to simulation results for validation of the KOT model and used to explain trends in the temperature history. The DSC crystallinity measurements are explained in section 4.3. The crystallinity measurements are compared to the result of the KOT simulation and crystallisation model, see subsection 4.3.1. The simulation model result is used to explain the difference in crystallinity for windings with small and large radiuses, the low crystallinity at the top and bottom surface and the presence of an initial crystallinity value.

4.1 LATW Specimens

The Carbon-PEEK rings created by Jasper Reichardt[7] are used to compare the thermal measurements and material properties with the results from the simulation model of this research. The thermal conditions were measured during the creation process of these rings, using multiple thermocouples to measure the thermal history of different layers. The material properties were later on investigated using DSC measurements for the crystallinity.

Two Aluminium 6082-t6 mandrels with a layer of Teflon tape[31] were used with the tape placement machine. The program was set-up for windings of sets of two plies in continuous succession. After doing so, the machine then cuts the tape, shuts down the laser and moves to its starting position (away from the mandrel). This allows for human inspection and insertion of thermocouples to take place, while also providing time for the material to cool down. The winding process is resumed only after the material has cooled to approximately equilibrium temperature[7].

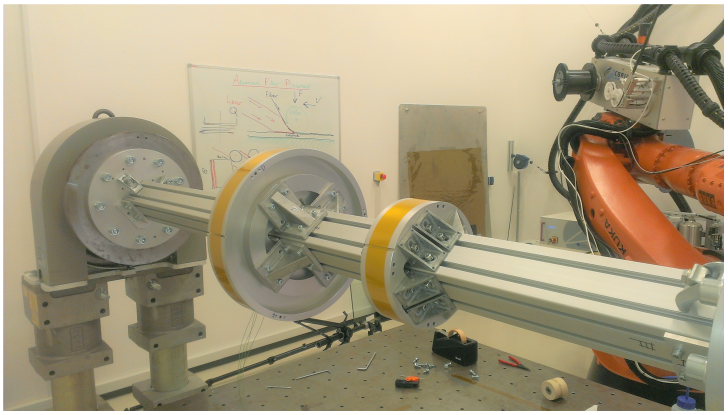

FIGURE 4.1: Aluminium mandrels for tape winding, radius of 122mm and 212mm

4.2 Thermocouple results

Thermocouple measurements temperatures over time are plotted (blue line) for lay-up on the 122mm and 212mm aluminium mandrels in respectively figure 4.2 and figure 4.3. The graph measures the thermal history of a specific layer at a single point.

To determine the difference between reality and the simulation, the KOT 3D simulation model 2C(see figure 2.17) has been used. The model used the global settings, but with an extra time delay between every two layers to simulate the longer cooling time between the sets of two plies as compared to the experiments. The KOT 3D simulation is plotted by the green line in figure 4.2 and figure 4.3.

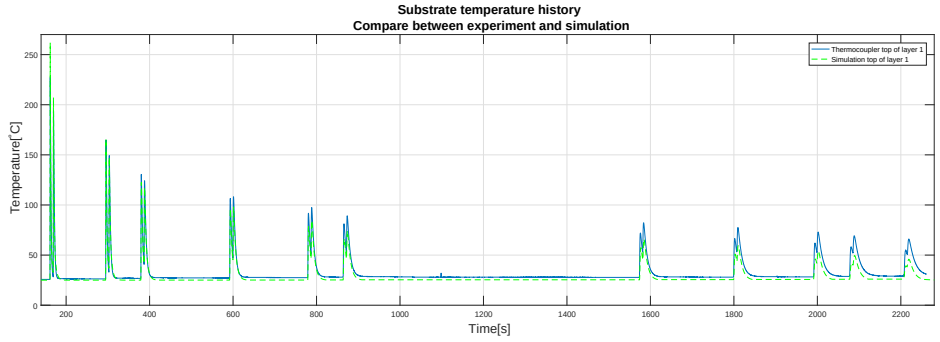

FIGURE 4.2: First layer thermocouples measurements and simulation results with a radius of 122mm.

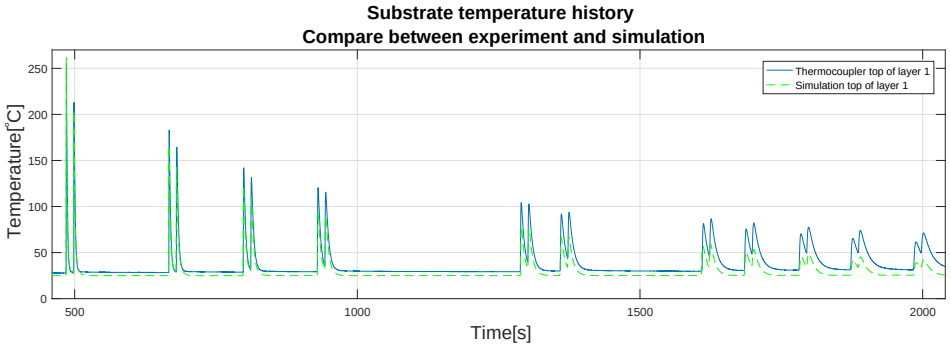

FIGURE 4.3: First layer thermocouples measurements and simulation results with a radius of 212mm.

4.2.1 Temperature development of experiments and simulations

The experiments measurement and the 3D simulation show minor differences in thermal history. The differences are indicated and explained in the following chapter.

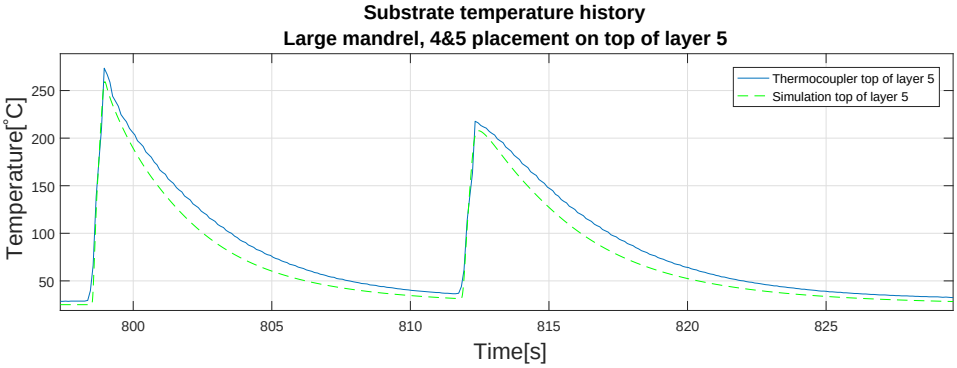

FIGURE 4.4: General curve difference

Between the thermocouple measurement and the simulation results, there is a notable difference in thermal history. Figure 4.4 illustrates this difference in cooling rate and higher peak temperatures. This is believed to be due to the effect of the roller and the perfect bonding condition between the substrate and mandrel.

4.2.2 Trend of peak temperatures in continuous hoop winding

In figure 4.2 and 4.3 we notice a change in trend, where the next hoop winding has a higher temperature than the previous winding. In figure 4.5, the trend change is shown by the 11th layer of the large mandrel. It occurs at a consecutive placement of the 6th and 7th layer on top of the 11th layer. The heat in the layer does not dissipate to the environment or equipment, before the next hoop winding which causes the trend change. The trend change occurs faster with a smaller mandrel or with a thicker substrate. The reason for this is that the heat of windings on a smaller mandrel have less time to dissipate, whereas on a thicker substrate the heat loss through conduction is lower. This trend is observed in the experiments as well as in the KOT simulation model.

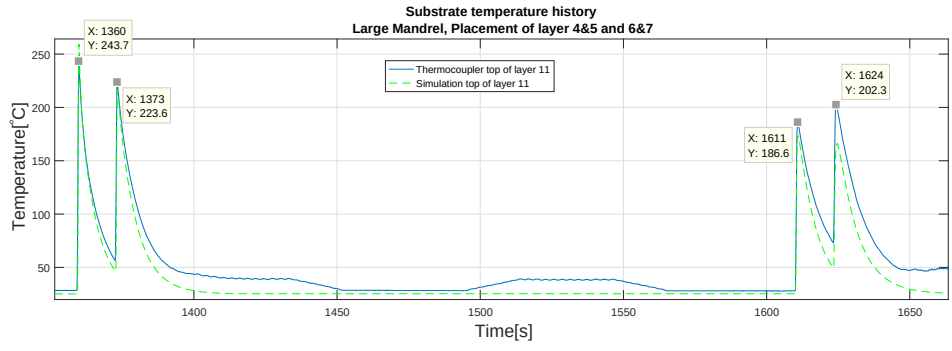

FIGURE 4.5: Trend change in thermocouples measurements and simulation results with a radius of 212mm.

4.2.3 Environment difference between experiments and simulation

Due to the set-up of the experiment in a closed environment, we notice heating of the equipment. This temperature increase is not lost to convection to the environment since the closed environment is also heating up. This is visible in the magnification of the temperatures between 20-35 °C of the large radius, seen in figure 4.6. The increase for the small radius is about 3°C, while the increase in environment temperature is 6 °C. Basically environmental temperatures during the experiment went up, whereas the simulation kept constant temperatures.

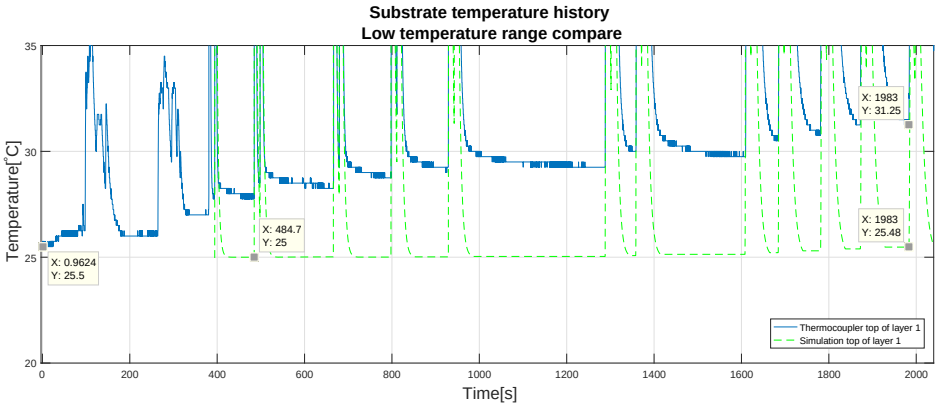

FIGURE 4.6: Temperature change in equipment.

4.3 Crystallinity measurements

The crystallinity percentage was measured of the Carbon fibre/PEEK composite rings using the Mettler Toledo DSC for multiple layers. The material was extracted using the position of the thermocouple and then cutting along the layer, subsequently extracting the material at a position away from the thermal influence of the thermocouple. This was performed for the 122mm and 212mm radius rings.

(A) Carbon-Peek ring.

(B) Mettler Toledo Digital Scanning Calorimetry

FIGURE 4.7: DSC Material and Equipement

The following equation was used to calculate the degree of crystallinity, X_C:

$$X_C = \frac{\Delta H_m - \Delta H_c}{\Delta H_f (1 - \alpha)} \tag{4.1}$$

where ΔH_m and ΔH_c are the enthalpy of fusion at melting point (integration above the endothermic peak), and the enthalpy of crystallisation (integration under the exothermic crystallisation peak), respectively. The enthalpy of fusion ΔH_f of fully crystalline PEEK is taken as 130 J/g [32], which is reduced by the mass fraction α of carbon fibre in the composite.

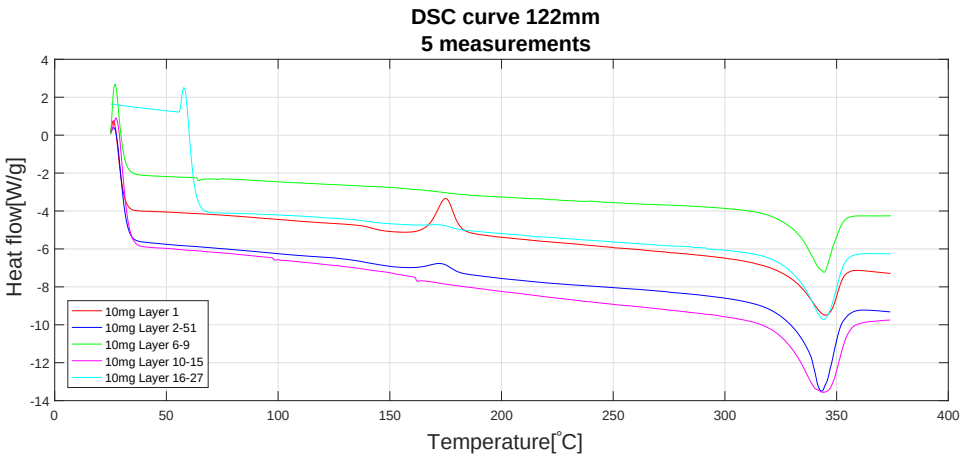

FIGURE 4.8: DSC curve for the 122mm radius ring.

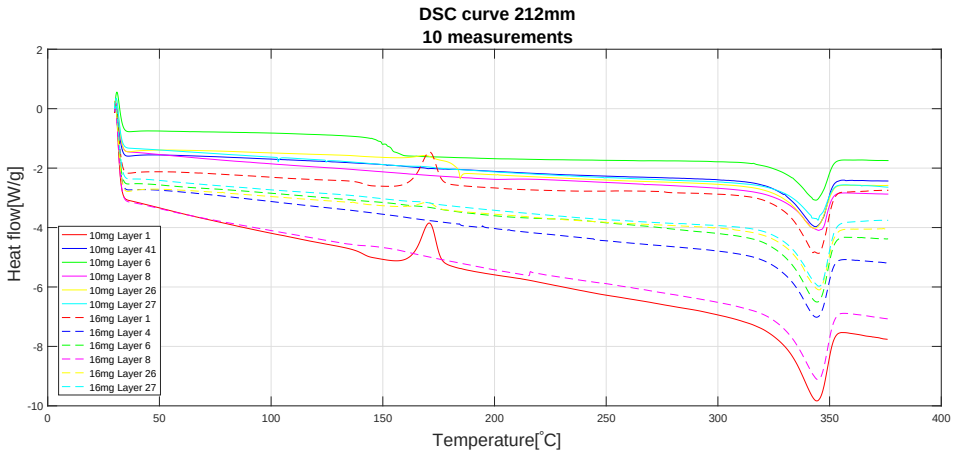

FIGURE 4.9: DSC curve for the 212mm radius ring, measurement performed by L. de Weert.

4.3.1 Crystallinity results

Using the equation 3.1 for the degree of crystallinity, the crystallinity was calculated from figure 4.8 and figure 4.9, of the small and large radius of the mandrel. The crystallinity results are as follows see table 4.1 and 4.2. The crystallinity of KOT simulation was calculated using the crystallinity model of chapter 3. In figure 4.10 is the crystallinity result of plotted every layer for the small radius(122mm) and large radius(212mm).

TABLE 4.1: Small radius DSC Results

	Layer 1	Layer 2-5	Layer 6-9	Layer 10-15	Layer 16-25
Crystallinity	23.03%	28.78%	28.69%	21.04%	26.01%

TABLE 4.2: Large radius DSC Results

	Layer 1	Layer 4	Layer 6	Layer 8	Layer 26	Layer 27
Crystallinity	26.34%	26.62%	27.13%	27.19%	25.49%	23.81%

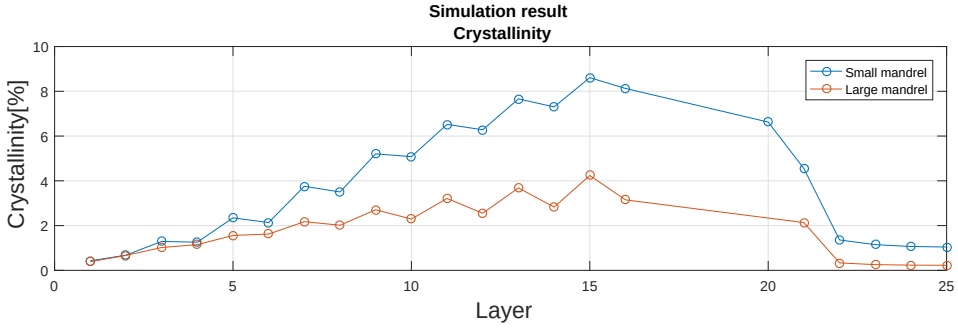

FIGURE 4.10: Simulation Crystallinity result, KOT model, hoop winding 2C

4.3.2 Crystallinity change per position

One of the objectives was the '**Prediction of the temperature depended material properties based on the heating and cooling history during manufacturing.**' the result of this is shown in figure 4.10 for the crystallinity growth during the LATW process. From the analyses of the results, the following can be concluded:

Lower crystallinity at the bottom and top in the results of the DSC measurements and Simulation model. Higher cooling rates are responsible for the lower crystallinity at the bottom since the conduction to the mandrel is much higher in comparison of the conduction to the laminate layers. With an aluminium mandrel, the conduction will be high for the first few layers, which results in higher cooling rates and consequently lower crystallinity. The higher cooling rate is also indicated in the DSC measurements of figure 4.8 and 4.9 for which the first layer showed an exothermic crystallization peak (first peak visible between 150-180°C), showing that crystallinity can still be formed even at low temperatures.

The difference in crystallinity values between the DSC measurements and Simulation model is the result of an unknown initial crystallinity percentage at nip-point. Since the material is only melted for a short duration(less than 1 second) and is almost fully crystallized at the start, it will not have enough time to become fully amorphous. This initial crystallinity is estimated to be should around 20-25%, which when added to simulation would result in similar values as the DSC measurements. This is confirmed by the presence of an exothermic crystallisation peak for the first layers in the DSC measurements of figures 4.8 and 4.9. The exothermic crystallisation peak is present since 'almost' no crystallisation growth occurred during the tape winding, due to the high conduction value of the aluminium mandrel.

The lower crystallinity at the top is simply because the top layer has experienced less heating/cooling cycles compared to the lower layers. If we examine the top surface it will only experience the placement, which has higher cooling rate because of the convection to air.

The fluctuation of higher and lower crystallinity in figure 4.10 is a result of the manufacturing set-up. The simulation and experiments were set-up to perform two hoop windings follow by a time delay. This resulted in that the layer of the first winding has a higher initial temperature and thus greater enthalpy and slightly lower cooling rates. This winding set-up resulted in a difference 0.05-0.5% for each uneven layer number.

The difference in crystallinity between the radius of 122mm and 212mm is also due to the manufacturing set-up, by performing two consecutive hoop windings will the initial temperature be higher for every second cycle. This initial higher temperature leads to more crystallinity growth for all layer since the crystallinity growth is affected by multiple heating and cooling cycles see chapter 3. The effect of higher initial temperature due to the previous cycle is less present in the large radius since the cooling cycle is almost twice as long as compared to the small radius. This initial temperature due to manufacturing set-up resulted in a difference up to 4% in crystallisation growth.

Chapter 5

Simulation Study

The simulations settings of section 2.12 are studied in this chapter. In section 5.1 are the different transverse boundary conditions studied by using the models of figure 2.17, in order to determine the geometry and boundary conditions that affect the material quality. To predict the effect of manufacturing set-up the following studies are preformed: the effect of tape width in sections 5.2 , change in radius in section 5.3 for hoop and adjacent winding, influence of mandrel material in section 5.4, occurrence of thermal degradation in section 5.5 and increased manufacturing temperature for environment, tooling and substrate in section 5.6. Consequences of LATW on various fibre-orientated substrates is studied in section 5.7.

5.1 Model Case Study

In in this section is **investigation of change in temperature history, as a result of transverse boundary conditions in width direction**. The transverse effects were reduced to perform this investigation, see the models in figure 2.17. Each of the models is compared to one another to determine the loss in data and effects this has on the thermal history.

5.1.1 Reduction in the adjacent winding model

In the first simplification we compare a simulation model with a width of five windings, we place 3 adjacent windings in the centre so that there are substrate and mandrel elements to the sides. This model is compared to a reduced version that does not have the extra substrate and mandrel elements on sides.

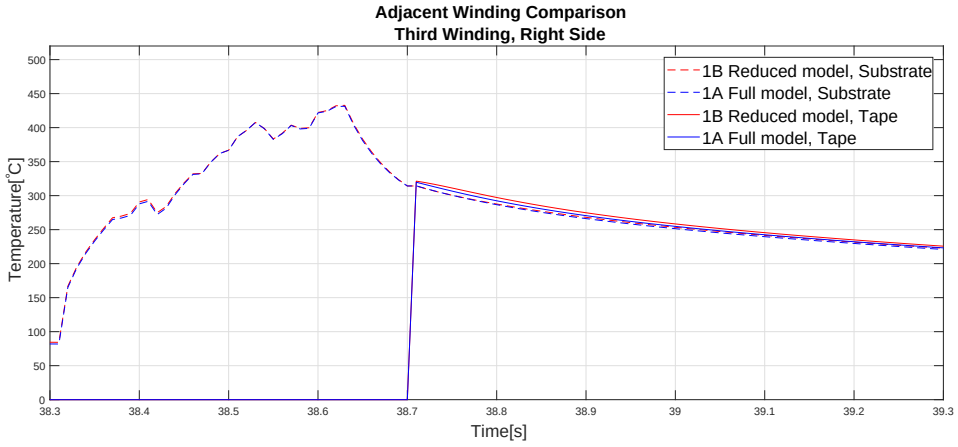

FIGURE 5.1: Reduction in adjacent winding model, Temperature around nip-point, KOT simulation, models 1A and 1B

In figure 5.1 is temperature history of the third winding, the first layer on the right sides edge is depicted. Here the difference in models is most appeared. There is a slight difference in the cooling rate slope after nip-point, this due to the increased conductivity to the sides of the substrate. This slight difference is only present in the left and right sides of respectively of the first and last adjacent winding, at the other positions in the tape can this difference be neglected. This influence on the first and last adjacent winding is comparable to the difference between the models 2C and 2A, see table 5.1.

5.1.2 Adjacent winding compared to hoop winding model

When comparing the adjacent winding to the hoop winding model, there is a difference in heating up of the system. Hoop winding will lead to the system heating up, because of consecutive placement at the same spot within a relatively short duration. This can be prevented by applying a time delay, but there is still data lost about the influence that adjacent windings have on another, this is further examined in subsection 5.3.2 using different mandrel radiuses.

5.1.3 Hoop winding model influence of substrate

Between the models 1B and 1A there is almost no change in temperature nip-point (>1°C) and negligible difference in temperature after the cooling cycle and crystallinity growth, see table 5.1. However this is performed for low transverse conductivity with 90°angled substrate, and since the transverse conductivity is increased for other laminate angles could this still have an effect. This is therefore further researched in section 5.7, by changing the substrate fibre-orientation.

5.1.4 No transverse convection and conduction

Removing the convection on the sides reduces the KOT simulation model, to essentially to a 2D model since all transverse effects in width direction are removed. From table 5.1 it can be seen that removal of the side convection has the largest effect, see the data of 2C and 2D. Not much difference in nip-point temperature (>2°C), but a relatively large difference of 1% in crystallinity and 7°C in cooled down temperature after the cycle. Especially the cooled down temperature will influence the crystallinity growth when more layers are wound. Side convection on the substrate also influences the tape more at the edge. Further research on influence on the edge is in section 5.2.

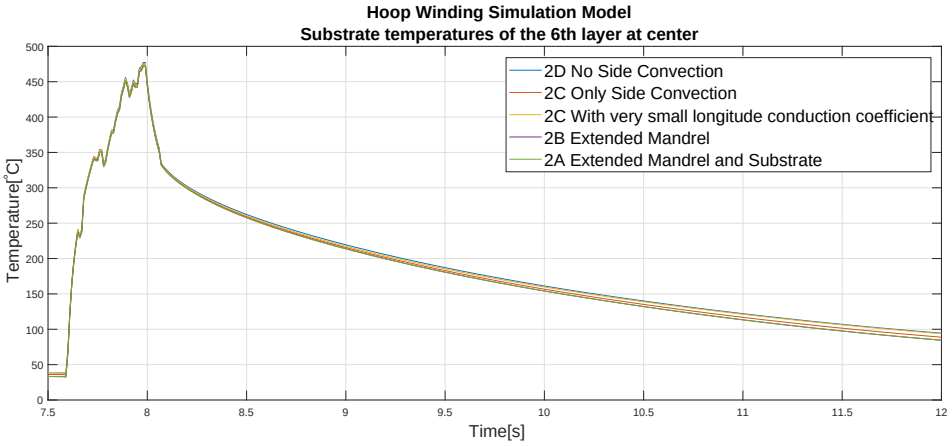

FIGURE 5.2: Change in Boundary Conditions in transverse direction, KOT simulation, Hoop winding models 2A, 2B, 2C and 2D.

TABLE 5.1: Data of different models of the 6th layer at center

Model	2D	2C	2B	2A	2C 'almost' no longitude
Nip-point Temperature	334.8°C	333.1°C	332.3°C	332°C	333.8°C
Cooled Temperature	54.35°C	47.88°C	43°C	42.95°C	51.88°C
Crystallinity	1.8429%	0.92%	0.7149%	0.7156%	1.15%

5.2 Variation in tape width

Tape winding can be done in width range of application ranging from the small to large manufacturing. Large manufacturing generally uses wider tape, while precision mechanics requires smaller tape to be placed for more detail. To examine the influence we variate the width geometry parameter w_t and w_s of the tape and substrate to determine the effect on temperature development with the KOT simulation. The tape width geometry parameter is simulated for 3mm, 6mm, 12mm, 24mm, 48mm and 96 mm, using the 3D simulation model with side convection and mandrel.

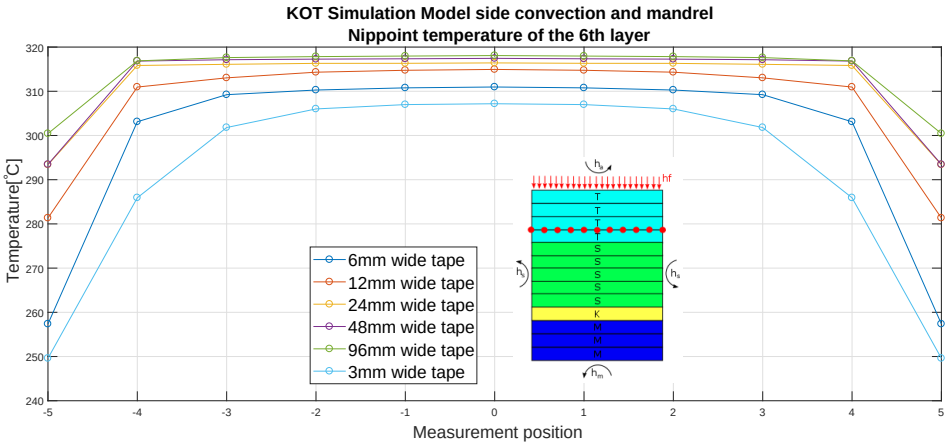

FIGURE 5.3: Nip-point temperature in transverse direction of multiple tape widths

In figure 5.3 shows the nippoint temperature of the six tapes. The influence that side convection has on the temperature on edge of the tape is clearly visible ranging from 15°C for wide tapes to even 55°C for smaller tapes. Side convection also influences the cooling rate of the tape, resulting in reduced crystallinity at the edge of the tape, see figure 5.4. The simulation results show that 3mm at edge the crystallinity is reduced through side convection.

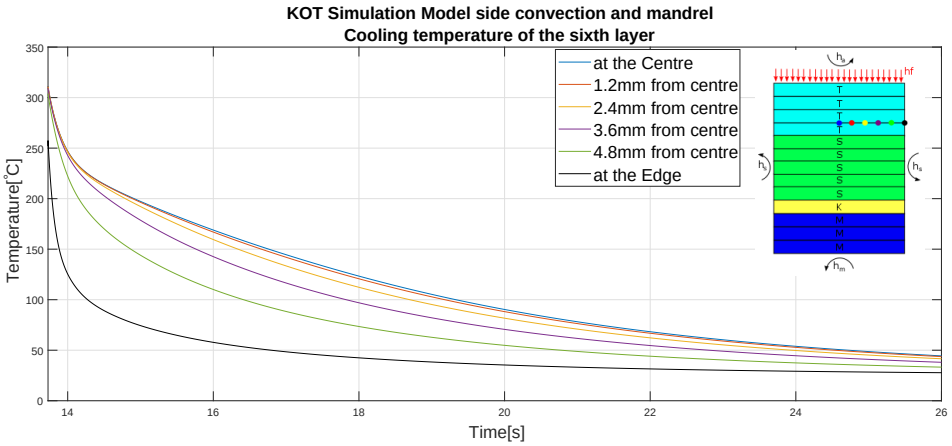

FIGURE 5.4: Cooling difference between centre and edge of a 12mm wide substrate

5.3 Variation in radius

5.3.1 Radius effect on hoop winding

The radius geometry parameter also has a lot of influence on the temperature, this is especially the case for hoop winding. The decrease in radius leads to a shorter of time available for cooling, for consecutive hoop windings. We researched the effect of radius change for two models, the 3D adjacent winding model and hoop winding mandrel model.

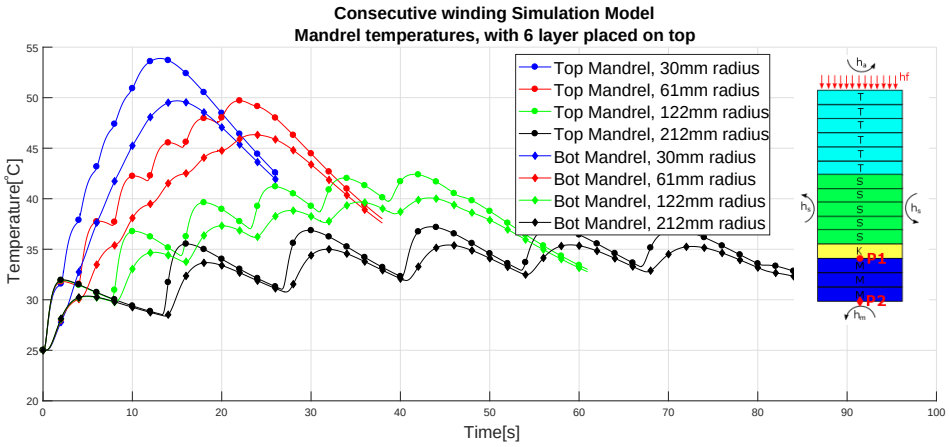

FIGURE 5.5: Mandrel temperature, hoop winding mandrel model

The mandrel is the most significant source of heat dissipation, this is due to through high convection at the bottom of the aluminium mandrel. But when the radius is decreased in hoop winding the heat will have less time to dissipate from the mandrel to air. Resulting in an increase in nip-point temperature of the substrate. In figure 5.5 the mandrel temperature is increased more with shorter hoop windings, this is due to the shorter time intervals between winding, for which the mandrel to air convection can't keep up. But even when the mandrel is acting a heat sink(fixed temperature at mandrel bottom) does the increase in temperature still occur, the conduction of the substrate to the mandrel is then the lagging factor, see figure 5.6.

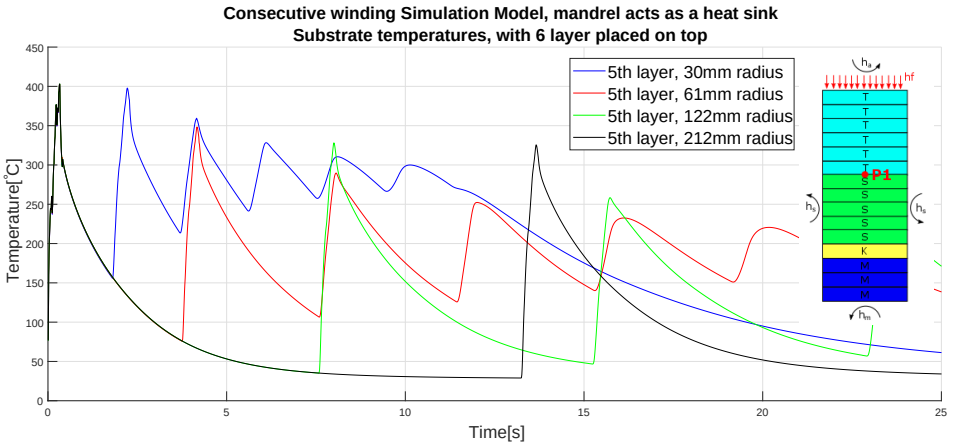

FIGURE 5.6: Substrate temperature, mandrel acts as a heat sink, hoop winding mandrel model.

5.3.2 Radius effect on adjacent winding

The radius has also been varied for adjacent windings, for 30mm, 60mm and 122mm. We will look at the thermal effect that adjacent windings have on one another. Since the cooling time is decrease more heat will remain in the previous adjacent wind to effect the placement.

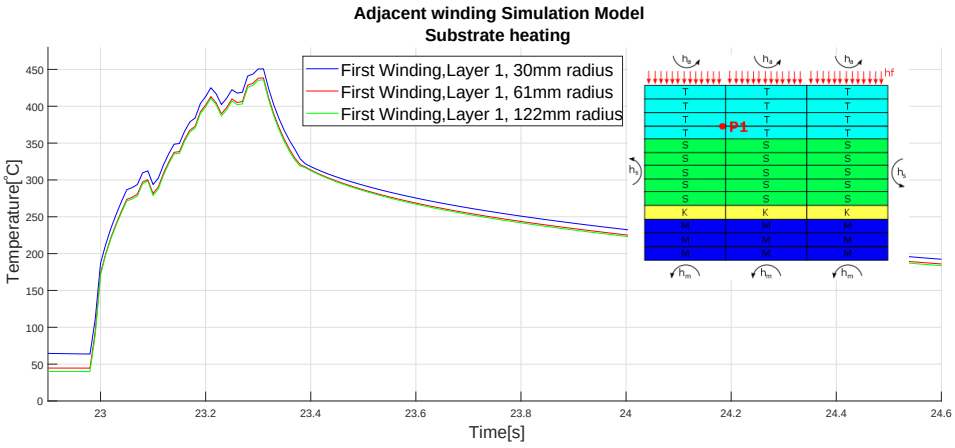

FIGURE 5.7: Radius change in adjacent winding, temperatures of the right side of the first winding

From the simulations in figure 5.7 it concludes that radius change only has an impact on the edge of the layer, 8°C in nip-point temperature for the 30.5mm as compared to the 61mm radius. On the centre the difference is slight >1°C. The reason for this is because of the high heat conductivity to the aluminium mandrel and low transverse conductivity. The heat has almost entirely dissipated in the previous adjacent wind. Which causes the influence on adjacent windings to be minimal. To study the influence mandrel conduction by a thermoplastic mandrels we will look to section 5.4 and for transverse conductivity section 5.7.

TABLE 5.2: Mandrel material properties

Material	Specific heat $J/(kg°C)$	Density Kg/m^3	Conductivity $W/(m°C)$
Steel	50	7850	500
Aluminum	172	2710	894
PEEK[33]	0.35	1310	1090

5.4 Mandrel material

The mandrel is the largest source of heat dissipation, especially the aluminum mandrel which uses relatively high conduction values and reacts in a way as a heat sink. In the following KOT simulation, we changed the material of the mandrel to following to steel, aluminum and PEEK see table 5.2. From figure 5.8 we see the influence of slow heat dissipation that a thermoplastic mandrel has on hoop winding. To make thermoplastic mandrels a viable option then hoop windings should not occur or with an increased time delay of more than one minute between one another to not have an effect.

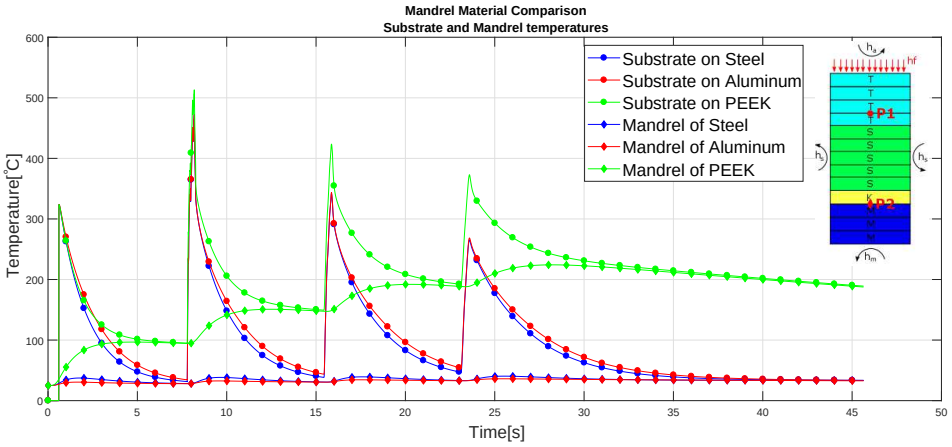

FIGURE 5.8: Effect of mandrel material on LATW

5.5 Thermal Degradation

Pyrolysis of Carbon-PEEK starts at a temperature of 450°C and at just under 600°C does the thermal degradation occur that would result in a rapid and significant mass loss. Normally only pyrolysis will occur for a very short duration in the first cycle as tape and (>0.5s) in the second cycle as substrate. Thermal degradation will normally not occur. Only with multiple consecutive hoop windings could this temperature be reached, and this would then also result in high nip-point temperatures, and thus bad bonding quality.

TABLE 5.3: Nip-point temperature and Crystallinity by different environment temperatures

Environment Temperature	25°C	35°C	45°C	55°C	65°C
Nip-point Temperature	334.8°C	338.1°C	341.5°C	344.9°C	348.3°C
Crystallinity	1.26%	1.94%	2.90%	4.17%	5.77%

5.6 Variation in environment temperature

Tooling and environment temperature influence the cooling rate. For the hoop winding on the mandrel model we will increase initial temperature of the tooling, environment and substrate, to determine the effect on Nip-point and crystallinity. The simulation was preformed with initial and environment temperatures of 25°C, 35°C, 45°C, 55°C and 65°C. The temperature of the substrate heating is compared in figure 5.9

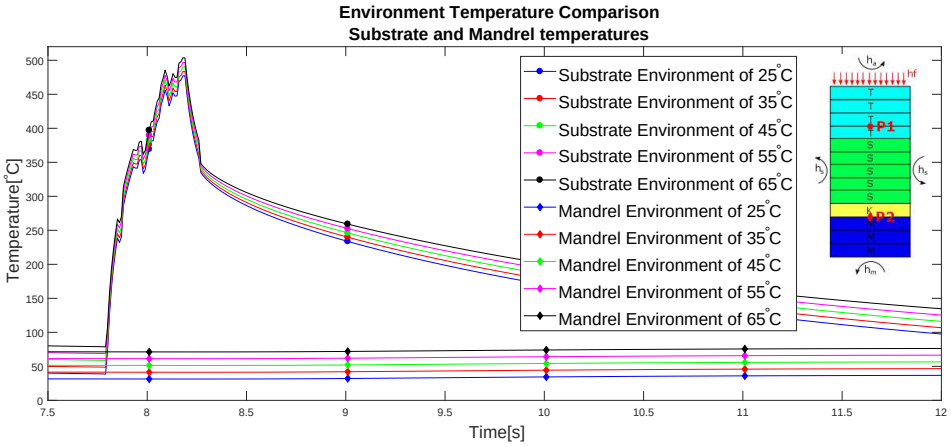

FIGURE 5.9: Effect of Environment Temperature on LATW

In figure 5.9 we only notice a slight increase in nip-point temperature as compared to the environment temperature. While we see a significant decrease the cooling rate. In table 5.3 is the data nip-point and calculated crystallinity using the model of chapter 3. We see that the nip-point increases with around 3.5°C per 10°C increase in environment temperature. Due to the decrease in cooling rate, we see an exponential increase crystallinity growth[1]. This leads to believe that increasing the tool and environment temperature to be viable option to promote crystallinity growth during LATW, more research in this is still necessary to determine the effect on the bonding between layers.

[1]Note that the crystallinity growth of this layer is based on the thermal history of four windings.

TABLE 5.4: Crystallinity of multiple width positions with different substrate fibre-orientations

Tape width position	Centre	4mm off edge	2mm off edge	Edge
Lay-up 0°	0.78%	0.63%	0.15%	0.003%
Lay-up 45°	0.86%	0.77%	0.28%	0.003%
Lay-up 90°	0.90%	0.88%	0.66%	0.0033%

5.7 Substrate Fibre-orientation

The consequences of lay-up on the heating and cooling cycle was researched, by tape winding on different fibre-orientated substrates. This study determines the effect that it will have on nip-point temperature and crystallinity. The same optical/heat flux data was used for all lay-ups to simplify the comparison. Winding on 0°, 45°and 90°fibre-orientated substrates was researched. Four layers of tape were wound around with a 90°angle, with the hoop winding method of KOT model 2A. Figure 5.10 shows the temperature history of the substrate close to the edge of the tape.

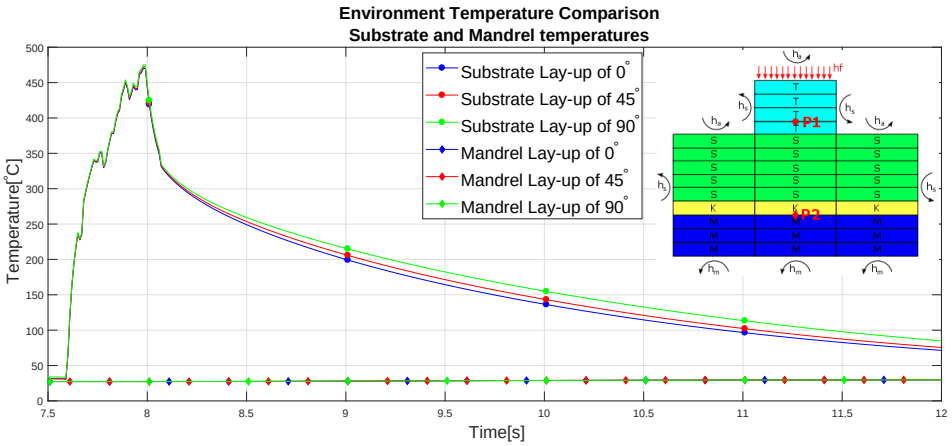

FIGURE 5.10: Influence by Lay-up on thermal history in LATW

There is only a slight difference in nip-point temperature >2°C at the edge and this decreases further to the centre. The same is the case for the cooling rate. Table 5.4 shows the difference in crystallinity in width direction of the tape. At the edge is almost no crystallinity growth, because of high cooling rates through air convection. Close off the edge the tape on 90°has higher crystallinity, but closer to the centre this difference reduced. This leads to the conclusion that the angle of the substrate has a slight effect(>1%) on crystallinity near the edge of the tape.

5.8 Evaluation

One of the conclusions we could draw from the **Investigation of change in temperature history, as a result of transverse boundary conditions in width direction**, was that all models showed at least some effect on the temperature history, but that combination of parameters is needed for some models to be of interest. The choice of model depends on one of the following conditions:

- Adjacent winding with extra substrate, KOT model 1A, small radius <60mm, 0°- 45°fibre-orientation substrate.
- Adjacent winding with extra substrate, KOT model 1B, small radius <60mm
- Hoop winding with extra substrate and mandrel, KOT model 2A, 0°- 45°fibre-orientation substrate.
- Hoop winding with mandrel, KOT model 2B, standard option
- Hoop winding only side convection, KOT model 2C, Thick substrate >10 layers
- Hoop winding no transverse bc's, KOT model 2D, Tape width >24 mm

Side convection and conduction have a smaller effect on nip-point than on cooling rate. For the nip-point temperature, only 1mm is effect at the edge with around 10-50°C of difference compared to the rest of the tape[2]. The cooling rate affects up to 3mm at the edge, resulting in 'almost' no crystallinity growth at the edge.

In researching **The consequences of lay-up on the heating and cooling cycle**, for heat absorption of the substrate and accumulated heat in the substrate and mandrel, the following was concluded in this chapter:

Pyrolysis of 450°will only occur for a duration of 0.5s in the first and second cycle. Thermal degradation will normally not occur, only in special cases such multiple consecutive hoop windings on a mandrel/substrate with low conduction value. This was the case for a PEEK mandrel of figure 5.8, the third layer reached a temperature above 600°C during the winding of the fourth layer for a short duration(>0.5s). Therefore care should be taken with the winding pattern to prevent consecutive windings on a 'non' conductive mandrel so that the system does not heat up.

For conductive mandrels, it could instead be an advantage to have more heat in the tooling and environment. Results showed that 4.5% more crystallinity growth is obtained with an increase of 40°C in tooling and environment temperature. Although this also resulted in an increase of nip-point temperature by 13.5°C, the nip-point temperature can be reduced by lowering the laser power. Lowering the laser power would also decrease the crystallinity, but there would still be more crystallinity growth present due to the change in cooling rate.

Substrate fibre-orientation showed for the cooling region only a slight difference in nip-point temperature >2°C at the edge and less than 1% crystallinity difference in the width direction. The heating region is more affected by the substrate fibre-orientation since this changes the optical settings.

[2]Note that the values calculated in this study are only specific to the global simulation parameters 2.1

Chapter 6

Conclusions and Recommendations

6.1 Conclusions

A three-dimensional Lagrangian transient simulation model and crystallinity model were created to for the prediction of the temperature depended material properties based on the heating and cooling history during manufacturing. The models were validated using experimental results and crystallinity measurements. From the experiment results and simulations model, occurring trends were discovered in the heating and cooling cycle. The change in trend was the point where the next hoop winding has an increasingly higher temperature compared to the previous winding. The reason for this was change conductivity with increased layers, this resulted in that the heat in the layer did not dissipate to the environment or equipment. The trend change occurs faster with a smaller mandrel or with more layers. The reason for this is that the heat of windings on a smaller mandrel has less time to dissipate.

From the DSC measurements and crystallinity model results it can be concluded that the second, third and fourth heating cycles are the most important for the crystallinity growth. Another conclusion was that it insufficient to only look at thermal history without taking the initial crystallinity percentage into account, otherwise only the crystallinity growth can be determined. Although with the value of crystallinity growth during the process a great deal can be explained, such as the difference in crystallization through-thickness or crystallinity difference between the radiuses. The most significant difference was up to 8% of crystallinity growth due to substrate conductivity change for the bottom layer, 6% due to less heating and cooling cycles for the top and 4% crystallinity growth difference due to the manufacturing set-up between radiuses.

An investigation of change in temperature history, due to effects of transverse boundary conditions was performed using a reduction of the transverse complexity in width direction. From this investigation, it was concluded that all models showed at least some effect on the temperature history, but that combination of parameters is needed for some models to be of interest. The difference between transverse effects in width direction, with and without showed 3°C in nip-point and 1% crystallinity difference in growth at the centre of the tape. But at the edge were the transverse effect far more present with up to -50°C of difference in nip-point temperature and 'almost' no crystallinity growth.

With the developed KOT models the following effects were studied: effect of variations in width, radius, mandrel material, environment temperature and lay-up. Variation in width determined that there is a decrease in the quality at edges of the tape, 1mm at the edge is affected by lower nip-point and up to 3mm at the edge is affected by a higher cooling rate and thus lower crystallinity growth.

Variation in radius showed that the system will heat up with consecutive hoop windings on an aluminium mandrel with a radius >122mm. This heating up of the system will lead to high nip-point temperatures so that no bonding can occur, but if the laser settings are instead lowered to compensate for the heating up of the system then the cooling rate will be lower, and thus more crystallinity growth. Results showed that 4.5% more crystallinity growth is obtained with an increase of 40°C in tooling and environment temperature.

Variation in substrate fibre-orientation showed negligible difference in nip-point temperature, but crystallinity growth was shown to be up to 0.5% lower.

6.2 Recommendations

6.2.1 Stress-Strain Model

The model is developed in shell131 elements which allow for node temperatures, it is possible to rerun the simulation with shell181 elements which allow for stresses and strains. The temperature input of the previous simulation can then be used for temperature depended stress-strain behaviour for the transient 3D LATW model.

6.2.2 After-treatment

To accurately predict the crystallinity based on the complex thermal history during LATW is a specialized and hard undertake, which would not achieve the result of directly improving the material quality. A method to directly achieve a higher crystallinity is by after treatment of the completed substrate. A test can be performed by heating the substrate to a temperature between Tg and Tm and then sustaining the temperature over different durations to promote the crystallinity growth. Measurements can then performed for the effect on crystallinity and bonding strength.

6.2.3 Winding Angle

Unfortunately, it was not possible to implement windings with diverse angles on top of the substrate within the time frame. Optical data was not available for more complex windings, as well as that the kinematic model and data collection would require a slight overhaul. The model with the current settings would also require additional elements, which would significantly increase the simulation time.

6.2.4 3D Transient model, no conductivity in placement direction

The model would inessentially still be a 3D thermal transient model, but with significantly fewer elements. The conductive area would be combination of different winding angles, for example: a tape with width direction 10 elements in consecutive placement would require just 10 elements, placement with 0° and 90° would then require an area of 10 by 10 elements, adding an angle of 45° leads to a octagon shape conductive area, continuing this for all angles leads to circle with a radius of 10 elements for the simulation model. The circle area can, of course, be curved according to the mandrel curvature.

6.2.5 Laser melt model

It turned out that the crystallinity of the tape did not become fully amorphous at melting temperature since the time spend at melt was less than 1 second. This of interest since the tape has a high initial crystallinity value before melt, and this research determined that the remaining crystallinity after melt primarily determines the final crystallization.

Bibliography

[1] L Sun, S. Mantell, D Banerjee, and D Cohen, "Thermoset winding process model and parametric study", *Proceedings of the ASME Materials Division*, vol. 69, no. 1, pp. 11–23, 1995.

[2] A. Barasinski, A. Leygue, E. Soccard, and A. Poitou, "An improvement in thermal modelling of automated tape placement process", *AIP Conference Proceedings*, vol. 1315, no. 1, pp. 185–190, 2011.

[3] C Brecher, A. Kermer-Meyer, and E., *Efficient processes for continuous fibre-reinforced themoplastics*, May 2014.

[4] A. consortium, "Amblifibre – adaptive model-based control for laser-assisted fibrereinforced tape winding", 2016. [Online]. Available: http://www.amblifibre.eu/.

[5] C. E. Commission, *ambliFibre Report Summary*. [Online]. Available: http://cordis.europa.eu/result/rcn/201148_en.html.

[6] W. J. B. Grouve, *Weld strength of laser-assisted tape-placed thermoplastic composites*. University of Twente, 2012.

[7] J. Reichardt, *Optical-Thermal Process Model for Laser-AssistedTape Winding*. University of Twente, 2016.

[8] J. Kim, T. J. Moon, and J. R. Howell, "Transient thermal modeling of in-situ curing during tape winding of composite cylinders", *Transaction-American Society of Mechanical Engineers Journal of Heat Transfer*, vol. 125, no. 1, pp. 137–146, 2003.

[9] J Kim, T. Moon, and J. Howell, "'effects of process variables on in-situ curing for thick composites using infrared heating", in *ASME International Mechanical Engineering Congress and Exhibition*, vol. 96, 1996, pp. 1–14.

[10] Y. M. Toso, P. Ermanni, and D. Poulikakos, "Thermal phenomena in fiber-reinforced thermoplastic tape winding process: Computational simulations and experimental validations", *Journal of Composite Materials*, vol. 38, no. 2, pp. 107–135, 2004.

[11] R. Akkerman, "'integrated process chain for automated and flexible production of fibre-reinforced plastic products", in *FIBRECHAIN Deliverable 3.4*, 2014.

[12] C. Stokes-Griffin and P. Compston, "A combined optical-thermal model for near-infrared laser heating of thermoplastic composites in an automated tape placement process", *Composites Part A: Applied Science and Manufacturing*, vol. 75, pp. 104–115, 2015.

[13] S. C. Dai and L. Ye, "Characteristics of cf/pei tape winding process with on-line consolidation", *Composites Part A: Applied Science and Manufacturing*, vol. 33, no. 9, pp. 1227–1238, 2002.

[14] S. Grove, "Thermal modelling of tape laying with continuous carbon fibre-reinforced thermoplastic", *Composites*, vol. 19, no. 5, pp. 367–375, 1988.

[15] J. Atkinson, J. Hay, and M. Jenkins, "Enthalpic relaxation in semi-crystalline peek", *Polymer*, vol. 43, no. 3, pp. 731–735, 2002.

[16] A. Van der Vegt and L. E. Govaert, *Polymeren: van keten tot kunststof*. VSSD, 2005.

[17] W. Wang, J. M. Schultz, and B. S. Hsiao, "Dynamic study of crystallization- and melting-induced phase separation in peek/pekk blends", *Macromolecules*, vol. 30, no. 16, pp. 4544–4550, 1997.

[18] C. J. Hilado, *Flammability handbook for plastics*. CRC Press, 1998.

[19] L. Perng, C. Tsai, and Y. Ling, "Mechanism and kinetic modelling of peek pyrolysis by tg/ms", *Polymer*, vol. 40, no. 26, pp. 7321–7329, 1999.

[20] P. Patel, T. R. Hull, R. W. McCabe, D. Flath, J. Grasmeder, and M. Percy, "Mechanism of thermal decomposition of poly (ether ether ketone)(peek) from a review of decomposition studies", *Polymer Degradation and Stability*, vol. 95, no. 5, pp. 709–718, 2010.

[21] A. Bejan, *Convection heat transfer*. John wiley & sons, 2013.

[22] A. Mechanical, "Theory reference", *ANSYS release*, vol. 14, 2011.

[23] P. A. D. Technologies, *The Focus - Issue 11*. [Online]. Available: http://www.padtinc.com/blog/wp-content/uploads/oldblog/PADT_TheFocus_11.pd.

[24] C. Carraher, *Seymour/Carraher's Polymer Chemistry: Sixth Edition*, ser. Undergraduate chemistry. CRC Press, 2003, ISBN: 9780824748647. [Online]. Available: https://books.google.nl/books?id=Jg_l8B7-4ngC.

[25] M van Drongelen, P. Roozemond, and G. Peters, "Non-isothermal crystallization of semi-crystalline polymers: The influence of cooling rate and pressure", *Polymer Crystallization II: From Chain Microstructure to Processing*, pp. 207–242, 2017.

[26] D. Blundell and B. Osborn, "The morphology of poly (aryl-ether-ether-ketone)", *Polymer*, vol. 24, no. 8, pp. 953–958, 1983.

[27] S.-L. Gao and J.-K. Kim, "Cooling rate influences in carbon fibre/peek composites. part 1. crystallinity and interface adhesion", *Composites Part A: Applied science and manufacturing*, vol. 31, no. 6, pp. 517–530, 2000.

[28] X. Tardif, B. Pignon, N. Boyard, J. W. Schmelzer, V. Sobotka, D. Delaunay, and C. Schick, "Experimental study of crystallization of polyetheretherketone (peek) over a large temperature range using a nano-calorimeter", *Polymer Testing*, vol. 36, pp. 10–19, 2014.

[29] M. Kuo, J. Kuo, M. Yang, and J. Huang, "On the crystallization behavior of the nano-silica filled peek composites", *Materials Chemistry and Physics*, vol. 123, no. 2, pp. 471–480, 2010.

[30] W. Wang, J. M. Schultz, and B. S. Hsiao, "Dynamic study of crystallization- and melting-induced phase separation in peek/pekk blends", *Macromolecules*, vol. 30, no. 16, pp. 4544–4550, 1997.

[31] D. Company, *Teflon PTFE Properties Handbook*.

[32] S.-L. Gao and J.-K. Kim, "Effect of cooling rate on interphase properties of carbon fibre/peek composites", *Journal of the Society of Materials Science, Japan*, vol. 48, no. 9Appendix, pp. 157–162, 1999.

[33] S. Z. Cheng, S. Lim, L. H. Judovits, and B. Wunderlich, "Heat capacities of high melting polymers containing phenylene groups", *Polymer*, vol. 28, no. 1, pp. 10 –22, 1987, ISSN: 0032-3861. DOI: https://doi.org/10.1016/0032-3861(87)90313-2. [Online]. Available: http://www.sciencedirect.com/science/article/pii/0032386187903132.

Appendix A

Method Comparison in LATP 3D simulation

A.1 3D Kinematic-Optical-Model for placement

The two simple model were developed for tape placement of a bowtie logo '⋈' using the two different methods. Data was collected for the method in different sizes and compared to one another to determine the best method for the 3D simulation.

A.1.1 Volume Solid70 elements

Simulation using the Birth and Death of elements, this method restricts the properties of death elements so that they do not take part in the simulation. New elements are birthed this simulates the placement of the tape, see figure A.1.

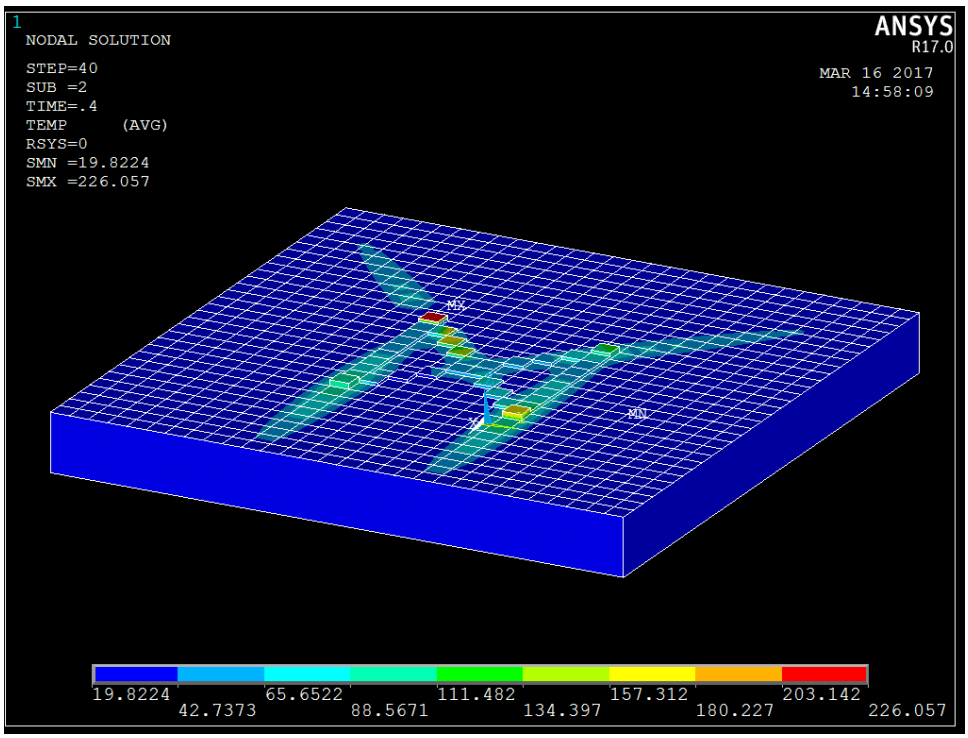

FIGURE A.1: LATP with Solid70 elements using Birth and Death of elements method

A.1.2 Section Shell131 elements

Simulation using Initial Conditions(IC's) simulation method, conditions are extracted for the previous result and are inputted as IC's for the next simulation. The section properties of the mesh will change at each time step to simulate the tape being placed, see figure A.2.

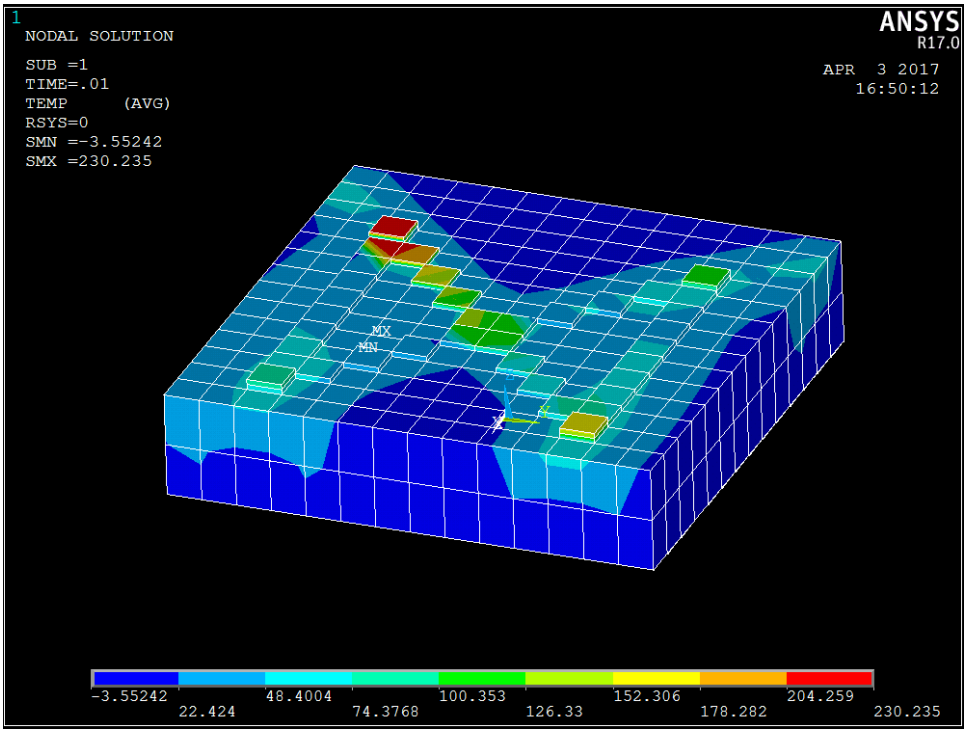

FIGURE A.2: LATP with Shell elements using the delevoped Initial Condition method

TABLE A.1: Method and Element comparison

Volume SOLID70 elements			
Surface area(mm)	30x30	60x60	120x120
Number of Elements	12600	21688	201600
Mesh time (s)	39	37	110
Simulation time (s)	274	698	2564
Section Shell131 elements			
Surface area(mm)	30x30	60x60	120x120
Number of Elements	2700	10800	43200
Mesh time (s)	25	42	80
Simulation time (s)	222	562	1895

A.2 Method Comparison

Both simulations use the same set-up, which is tape placement on a 3mm thick laminate, in the shape of '⋈' logo. Tape placement at a temperature of 280°C and heating with a equal distributed heat flux over and area of 10mm, and mandrel convection bottom and air convection at the top of the surface. Both have the same element size of 1 mm^2.

The model using Shell elements and Initial Condition method results in lower simulation times and less computational cost for the machine, see table A.1. With size increase the simulation time increase exponentially, therefore there is a need for local mesh refinement or model reduction, to prevent a time consuming simulation.

Appendix B

ANSYS Thermal Equations

B.1 Heat flow Fundamentals

Rewritten version of the heat flow fundamentals of Mechanical APDL Theory Reference[22]. Used for reference purposes through out the report.

B.1.1 First law of thermodynamics

The first law of thermodynamics states that thermal energy is conserved. Specialising this to differential control volume:

$$\rho c_p(\frac{\partial T}{\partial t} + v^T\{L\}T) = \{L\}^T[D]\{L\}T + \ddot{q} \tag{B.1}$$

ρ = density (input as DENS)
c = specific heat (input as C)
T= Temperature (=T(x,y,z,t))
t = time
$\begin{bmatrix}\frac{\partial}{\partial x} & \frac{\partial}{\partial y} & \frac{\partial}{\partial z}\end{bmatrix}^T$ = vector operator
{v}= velocity vector for mass transport of heat
{q} = heat flux vector (output as TFX, TFY and TFZ)
$\ddot{q}$ = heat generation rate per unit volume (input on BF or BFE commands)

Fourier's law is used to relate the heat flux vector to the thermal gradients:

$$\{q\} = -[D]\{L\}T \tag{B.2}$$

Where: $[D] = \begin{bmatrix} K_{xx} & 0 & 0 \\ 0 & K_{yy} & 0 \\ 0 & 0 & K_{zz} \end{bmatrix}$ = conductivity matrix
K_{xx}, K_{yy}, K_{zz} = conductivity in the element x, y, and z directions, respectively (input as KXX, KYY, KZZ on MP command)

Combining Equation B.1 and Equation B.2,

$$\rho c_p(\frac{\partial T}{\partial t} + v^T\{L\}T) = \{L\}^T[D]\{L\}T + \ddot{q} \tag{B.3}$$

Expanding Equation B.3 to its more familiar form:

$$\rho c_p(\frac{\partial T}{\partial t} + V_x\frac{\partial T}{\partial x} + V_y\frac{\partial T}{\partial y} + V_z\frac{\partial T}{\partial z}) = \frac{\partial}{\partial x}(K_{xx}\frac{\partial T}{\partial x}) + \frac{\partial}{\partial y}(K_{yy}\frac{\partial T}{\partial y}) + \frac{\partial}{\partial z}(K_{zz}\frac{\partial T}{\partial z}) + \ddot{q} \tag{B.4}$$

B.1.2 Boundary Conditions

It will be assumed that all effects are in the global Cartesian system. Three types of boundary conditions. It is presumed that these cover the entire element. Specified temperatures acting over the surface S1:

$$T = T* \tag{B.5}$$

, where T* is the specified temperature (input D)

Specified heat flows acting over surface S2:

$$\{q\}T\{\eta\} = -q^* \tag{B.6}$$

,where: $\{\eta\}$ = unit outward normal vector and q^*=specified heat flow(Input on SF or SFE)

Specified convection surface acting over surface S3 (Newton's law of cooling):

$$\{q\}T\{\eta\} = -h_f(T_S - T_B) \tag{B.7}$$

Where: hf = film coefficient this is evaluated at (TB + TS)/2 unless otherwise specified for the element (for example with heat flux, then it's at value of 1)
TB=bulk temperature of the adjacent fluid, TS=temperature at the surface of the model
(note that positive specified heat flow is into the boundary, so in the opposite direction of $\{\eta\}$, which accounts for the negative signs in Equations (6) and Equations (7)) Combining EQ(2) with EQ(6) and EQ(7):

$$\eta T[D]LT = -q* \tag{B.8}$$

$$\eta T[D]LT = hf(TB - T) \tag{B.9}$$

Premultiplying EQ(3) by a virtual change in temperature, integrating over the volume of the element, and combining with EQ(8) and EQ(9) with some manipulation yields:

$$\begin{aligned} &\int_{vol}(\rho c\delta T(\frac{\partial T}{\partial t} + \{v\}^T LT) + \{L\}^T(\delta T)[D]\{L\}T)d(vol) = \\ &\oint_{S2}\delta T q^* d(S_2) + \oint_{S3}\delta T h_f(T_B - T)d(S_3) + \int_{vol}\delta T\ddot{q}\,d(vol) \end{aligned} \tag{B.10}$$

where: vol= volume of the element and δT= an allowable virtual temperature (=$\delta T(x, y, z, t)$)

B.1.3 Derivation of Heat flow Matrices

As stated before, the variable T was allowed to vary in both space and time. This dependency is separated as:

$$T = \{N\}^T\{T_e\} \tag{B.11}$$

(11) where: $T = T(x, y, z, t)$= temperature $\{N\} = \{N(x, y, z)\}$ = element shape functions $\{T_e\} = \{T_e(t)\}$ = nodal temperature vector of element

Thus, the time derivatives of Equation A–11 may be written as:

$$\dot{T} = \{N\}^T\{\dot{T}_e\} \tag{B.12}$$

δT has the same form as T:

$$\delta T = \{\delta T_e\}^T N(13) \tag{B.13}$$

The combination LT is written as

$$LT = [B]T_e \tag{B.14}$$

where: $[B] = \{L\}\{N\}T$

Now, the statement of EQ(A–10) can be combined with EQ(A–11) thru EQ(A–14) to yield:

$$\begin{aligned}\int_{vol}(\rho c\{\dot{T}_e\}^T\{N\}\{N\}^T\{\delta\dot{T}_e\})d(vol) + \int_{vol}(\rho c\{\delta T_e\}^T\{N\}v^T[B]\{T_e\})d(vol)\\ + \int_{vol}(\{\delta T_e\}^T[B]^T[D][B]\{T_e\})d(vol) = \oint_{S2}\{\delta T_e\}^T\{N\}q^*d(S_2)\\ + \oint_{S3}\{\delta T_e\}^T\{N\}h_f(T_B - \{N\}^T\{T_e\})d(S_3) + \int_{vol}\{\delta T_e\}^T\{N\}\ddot{q}d(vol)\end{aligned} \tag{B.15}$$

Terms are defined in Heat Flow Fundamentals. ρ is assumed to remain constant over the volume of the element. On the other hand, c and $\ddot{q}$ may vary over the element. Finally, $\{T_e\}$,$\delta\dot{T}_e$, and $\{\delta T_e\}$ are nodal quantities and do not vary over the element, so that they also may be removed from the integral. Now, since all quantities are seen to be premultiplied by the arbitrary vector $\{\delta T_e\}$, this term may be dropped from the resulting equation. Thus, EQ(A–15) may be reduced to:

$$\begin{aligned}\rho\{\dot{T}_e\}\int_{vol}(c\{N\}\{N\}^T)d(vol) + \rho\{T_e\}\int_{vol}(c\{N\}v^T[B])d(vol)\\ +\{T_e\}\int_{vol}([B]^T[D][B])d(vol) = \oint_{S2}\{N\}q^*d(S_2)\\ +T_B\oint_{S3}\{N\}h_f d(S_3) - \{T_e\}\oint_{S3}h_f\{N\}\{N\}^T d(S_3) + \int_{vol}\{N\}\ddot{q}d(vol)\end{aligned} \tag{B.16}$$

EQ(A–16)may be rewritten as:

$$[C_e^t]\{\dot{T}_e\} + ([K_e^{tm}] + [K_e^{tb}] + [K_e^{tc}])\{T_e\} = \{Q_e\} + \{Q_e^c\} + \{Q_e^g\} \tag{B.17}$$

where:

$[C_e^t] = \rho\int_{vol}(c\{N\}\{N\}^T)d(vol)$=element specific heat(thermal damping) matrix

$[K_e^{tm}] = \rho\int_{vol}(c\{N\}v^T[B])d(vol)$=element mass transport conductivity matrix

$[K_e^{tb}] = \int_{vol}([B]^T[D][B])d(vol)$ =element diffusion conductivity matrix

$[K_e^{tc}] = \oint_{S3}h_f\{N\}\{N\}^T d(S_3)$ = element convection surface conductivity matrix

$\{Q_e\} = \oint_{S2}\{N\}q^*d(S_2)$= element mass flux vector

$\{Q_e^c\} = T_B\oint_{S3}\{N\}h_f d(S_3)$= element convection surface heat flow vector

$\{Q_e^g\} = \int_{vol}\{N\}\ddot{q}d(vol)$ = element heat generation load

B.2 Element Settings

The calculation of temperatures though thickness of shell elements is simplified version compared to volume elements, in regard to geometric complexity. With volume elements each corner or mid nodes have there own coordinates, with shell elements the calculation points in thickness direction only have distance to own another. This reduces the complexity of the geometry and thus simplifies the equation to be solved, resulting in faster calculation.

The temperatures in the rest of the Shell element 131 are a distributions of the internal temperatures that is visualized, this is done by a simply linear interpolation between the temperatures of the nodes.

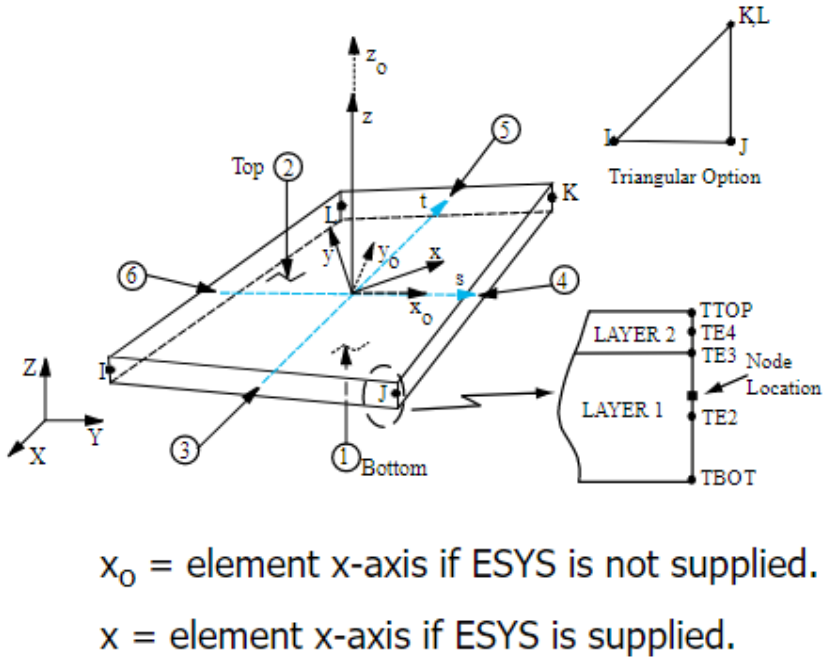

FIGURE B.1: Shell 131 Element

B.3 Convergence tolerances

The ANSYS program considers a nonlinear solution to be converged whenever specified convergence criteria are met. Convergence checking may be based on temperatures, heat flow rates, or both. You specify a typical value for the desired item (VALUE field on the CNVTOL command) and a tolerance about the typical value (TOLER field). The convergence criterion is then given by VALUE*TOLER. For instance, if you specify 500 as the typical value of temperature and 0.001 as the tolerance, the convergence criterion for temperature is 0.5 degrees. For temperatures, ANSYS compares the change in nodal temperatures between successive equilibrium iterations (T = Ti - Ti-1) to the convergence criterion. Using the above example, the solution is converged when the temperature difference at every node from one iteration to the next is less than 0.5 degrees. For heat flow rates, ANSYS compares the out-of-balance load vector to the convergence criterion. The out-of-balance load vector represents the difference between the applied heat flows and the internal (calculated) heat flows.

Appendix C

Constraint eq between shell elements

Shell elements are bit harder to connect to one another when they have different section properties, see figure C.1. Normally two elements share the same node at their intersecting position see C.1a. But when the elements have different amount of layer in their section properties compared to one anothe, then the temperature of the wrong layer is linked to one another, see C.1b. In here we see that of the right sided element the top temperature 'TTOP' of the second layer is matched with the top temperature of the third layer of the left sided element, while physically it should be matched with top temperature of the second layer of the left element 'TE3'.

This problem in Ansys is solved by using constraint equations to couple the two elements. To apply the constraint equation an additional node is necessary in the left sided element. By creating an additional node for the left sided element, then the standard method for matching elements can be evaded. A constraint equation equalizes the nodal values of the two elements to their corresponding layer, as seen in C.1c.

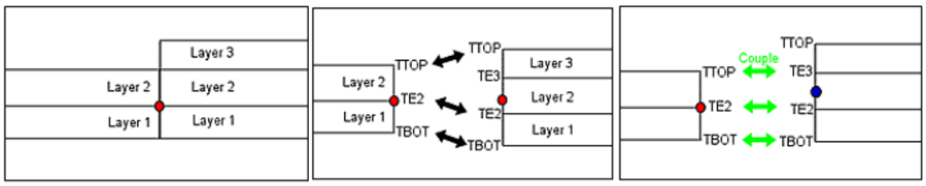

(A) Shared node (B) Standard coupling (C) Adjusted coupling

FIGURE C.1: Coupling of SHELL131 elements[23]

Appendix D

Reduced Model Validation

To validate the reduced 3D model, it is compared to the 3D full model. The reduced model only takes a smaller surface into account, and does a time skip to calculate the cooling history during the missing surface area. This can done because the situation reaches a steady-state, and thus providing no new data for the model, See figure X.x.A.

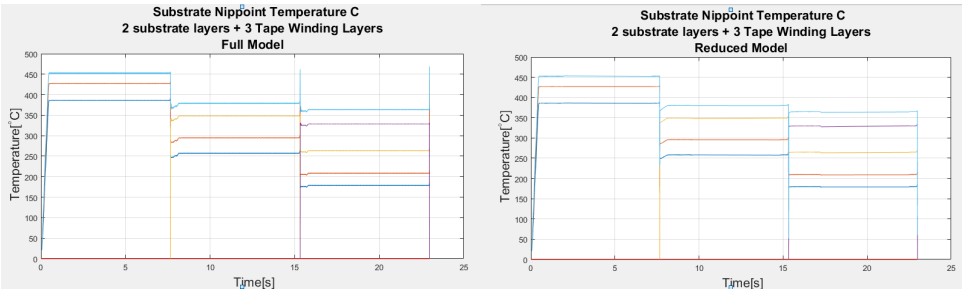

(A) Full perimeter (B) Reduced perimeter

FIGURE D.1: Nip-point temperatures, KOT adjacent 3B model

The Reduced model severely decreases the computation time of the model, while giving the same result for the area of interest.

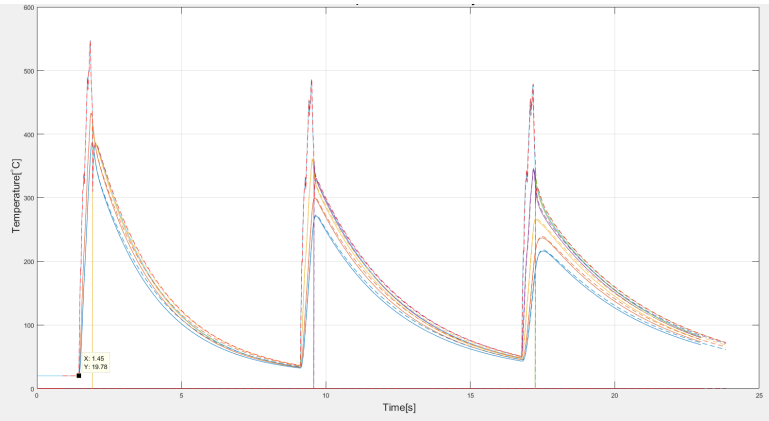

FIGURE D.2: Themperature history, full and reduced perimeter, KOT adjacent 3B model

Appendix E

Temperature depended material

E.1 Material Study

In previous research constant material values were used to determine the temperatures during laser assisted tape winding, with the new 3D simulation model it is possible to use temperate dependent material behaviour. We overview the effect of temperature depended material behaviour compared to fixed material values in LATW, using the material parameters of Table 2.4.

The simulation was run using the 2C hoop winding model that calculate the temperatures of the first placement on a 5 layer substrate at the center position. The comparison was made by changing only one material parameter to temperature depended at per simulation, with the rest of material parameters constant.

E.2 Simulation results

E.2.1 longitude, Transverse conductivity and Density

The influence of Kxx, Kyy and Density is less than 1°C, so this can be neglected.

E.2.2 Through thickness conductivity

The conductivity in thickness direction has more influence on the system, this is because most of the temperature is lost through the bottom and top surface.

The temperature depended increase in thickness-conductivity results in a lower heating temperature by the laser(-20°C), since the conductivity increase above 150°C than the standard comparison value of 0.72 W/(m °C). Which conforms with the heat equation of EQB.17, of which the $[K_e^{tb}] = \int_{vol}([B]^T[D][B])d(vol)$ =element diffusion conductivity matrix changes.

For temperatures below 150°C the material experiences less temperature loss due to conduction.

E.2.3 Heat Capacity

From the formula in EQB.17, $[C_e^t] = \rho \int_{vol}(c\{N\}\{N\}^T)d(vol)$=element specific heat(thermal damping) matrix it can be seen that the specific heat influence the rate of temperature change. At lower temperatures the specific heat has a low value, thus causing an increase in rate of temperature change. Which leads to the higher heating rate by the laser and the faster cooling rate, which can also been seen in figure E.2

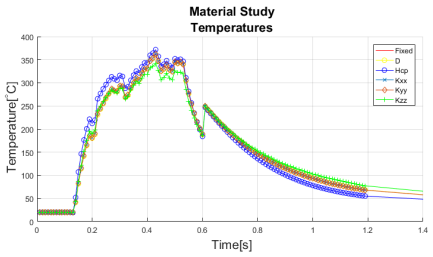

(A) Temperature History

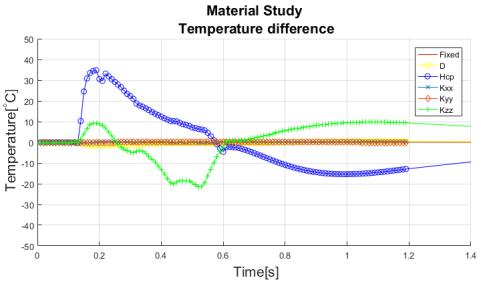

(B) Difference in Temperature

FIGURE E.1: Material Study: Temperature

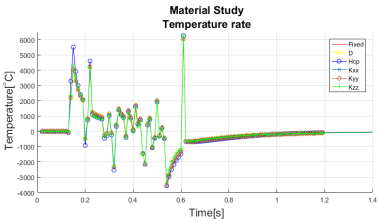

(A) Heating and Cooling Rate

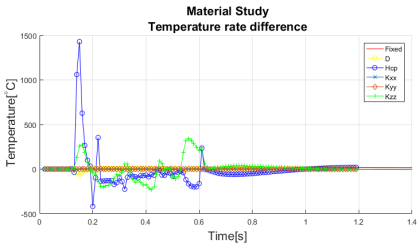

(B) Difference in Heating and Cooling Rate

FIGURE E.2: Material Study: Heating and Cooling Rate